Title
Multiple Modes of PV Interneuron Plasticity in Mouse Somatosensory Cortex

Author
Aman, Joseph

Publication Date
2022

Peer reviewed|Thesis/dissertation

Multiple Modes of PV Interneuron Plasticity in Mouse Somatosensory Cortex

By

Joseph W Aman

A dissertation submitted in partial satisfaction of the

requirements for the degree of

Doctor of Philosophy

in

Neuroscience

in the

Graduate Division

of the

University of California, Berkeley

Committee in charge:

Professor Daniel E. Feldman, Chair
Professor Frederic Theunissen
Professor Helen Bateup
Professor Marla Feller

Summer 2022

Abstract

Multiple Modes of PV Interneuron Plasticity in Mouse Somatosensory Cortex

by

Joseph W Aman

Doctor of Philosophy in Neuroscience

University of California, Berkeley

Professor Daniel E. Feldman, Chair

The cerebral cortex continuously adapts through learning and changes in sensory experience. A major goal of neuroscience is to understand the cellular and synaptic plasticity mechanisms that allow behavior to adapt to a changing environment. Remarkably, neural circuits maintain stable activity despite ongoing adaptive changes in synaptic strength and connectivity. Recent work has revealed multiple homeostatic plasticity mechanisms that maintain neural firing rates within an optimum range. However, it is not well understood how brain circuits maintain homeostasis in different brain regions and across different time scales.

In primary sensory cortex, changes in sensory input drive adaptive changes in cortical representations. Broadly, depriving a set of sensory inputs rapidly weakens neural responses to those inputs and gradually strengthens spared inputs. Recent studies show that deprivation also triggers rapid plasticity in inhibitory circuits that could stabilize neural activity despite ongoing weakening of deprived inputs. Chapter 2 investigates the cellular and circuit mechanisms that underlie this rapid plasticity of inhibition in the superficial layers of rodent primary somatosensory cortex (S1). This study shows that 1-day whisker deprivation weakens inhibition in layer (L) 2/3 pyramidal neurons by decreasing the intrinsic excitability of L2/3 parvalbumin-positive (PV) interneurons near spike threshold. Deprivation reduces PV spike threshold through an increase in voltage-gated potassium conductances. These findings demonstrate that activity in sensory cortex is rapidly stabilized through plasticity of PV intrinsic excitability.

Often, a single sensory manipulation drives multiple cellular and circuit changes with distinct temporal components. In cortical inhibitory circuits, the time course of plasticity is not well understood. Building on the studies in Chapter 2, we hypothesized that additional plasticity mechanisms may be recruited in L2/3 PV neurons in response to different time scales of whisker deprivation. In Chapter 3, we test this idea by extending the the duration of whisker deprivation to 3 days and asking whether changes in L2/3 PV circuits are consistent with those observed after 1 day of deprivation. We find that 3-day deprivation also decreases PV intrinsic

excitability, but through a different mechanism than 1-day deprivation. Deprivation strengthens the medium afterhyperpolarization (mAHP) without affecting spike threshold. Thus, experience-dependent plasticity of cortical PV circuits involves a succession of distinct components.

Table of Contents

Acknowledgements

This thesis would not be possible without the support of my friends, colleagues, and family. First, I would like to thank Dan for his patience and support over the years. Thank you for teaching me how to think carefully about scientific problems and interpret confusing data. Despite balancing so many roles, Dan is seemingly always available to offer help. Dan's commitment to mentoring serves as an example I hope to follow in my future work.

I'm grateful to have worked alongside many thoughtful and supportive labmates. Thank you to Melanie Gainey, whose work appears in this thesis, and Michelle Antoine for helping me with my early experiments. Thank you to Brian Isett, Sam Harding-Forrester, Amy LeMessurier, Kevin Laboy, Han Chin Wang, Deepa Ramamurthy, Bree Bohannon, Hannah Monday, Lucia Rodriguez, Kaeli Vandemark, and Laura Gomez. I would like to thank Tomer Langberg for being an endlessly supportive friend and labmate and for helping to make the lab a truly enjoyable place to work. Thanks also to all the wonderful folks next door in Marla Feller's lab. I would like to Sanika Ganesh for her help with experiments, and for putting so much careful work into an impressive undergraduate project. Thank you to our indispensable lab manager Katie Smith for helping with viral injections, ordering, surgical technique, and all things mouse related. To everyone in the Feldman lab, thank you for your feedback, guidance, and friendship.

Thank you to everyone in the Helen Wills community. I feel lucky to have met many creative and talented people who helped me think in new ways. Thank you to Candace Groskreutz, who was the HWNI program administrator for most of my time here. Thanks also to Dan Feldman and Michael Silver for overseeing the grad program. Thank you to the members of my thesis committee for their advice and feedback: Helen Bateup, Marla Feller, and Frederic Theunissen.

I would like to thank Mathew Summers and Gabriella Martini for their support and friendship. Thanks for being great housemates and for making the pandemic bearable through countless hours of conversation. Finally, I thank my parents, Ken and Debbie, and my sister Genasee for their unflagging encouragement and support over the years.

Chapter 1

Introduction

Neural circuits must maintain stable mean activity levels and some aspects of firing patterns while also adapting to changes in an organism's sensory environment. It remains unclear how the brain balances the competing demands of stability and flexibility. Neural circuits adapt to changes in input through Hebbian plasticity, in which correlated presynaptic and postsynaptic activity strengthens synapses, and uncorrelated activity weakens synapses. While Hebbian plasticity stores information about sensory patterns in neural circuits, it has long been recognized that Hebbian plasticity also destabilizes neural activity because of its positive feedback nature (Miller & MacKay, 1994). To prevent runaway activity or network quiescence, synapse-specific Hebbian mechanisms such as long-term potentiation (LTP) and depression (LTD) must be constrained by cellular-level homeostatic mechanisms (Zenke, Hennequin, & Gerstner, 2013). Clear evidence that cellular homeostatic mechanisms exist is apparent from the circuit-level phenomenon of firing rate homeostasis, in which a manipulation that should stably increase or decrease firing rate (e.g., continuous partial blockade of sodium channels) drives only a transient change in firing rate, that then spontaneously recovers back to baseline levels via an endogenous homeostatic process. In recent years, research has given a clearer picture of how neural circuits implement firing rate homeostasis (review: Pozo & Goda, 2010). However, our understanding of the cellular and circuit mechanisms that stabilize activity across different temporal and spatial scales remains incomplete.

The first description of a mechanism for firing rate homeostasis came from studies of neural activity in cortical cell culture (G. G. Turrigiano, Leslie, Desai, Rutherford, & Nelson, 1998; O'Brien et al., 1998). In these early studies, chronic pharmacological suppression of neural activity drove a compensatory increase in excitatory synaptic strength, whereas blocking inhibitory transmission had the opposite effect. This demonstrated that global, homeostatic changes in synaptic strength exist that have the potential to bidirectionally stabilize network activity. The mechanism underlying up-regulation of synaptic strength in these early experiments was termed synaptic scaling and was discovered to be mediated by changes in AMPA receptor trafficking to the postsynaptic membrane that increased AMPA receptor

numbers at synapses (Gina G. Turrigiano, 2008). Likewise, synaptic down-scaling was found to reflect decreased AMPA receptors at synapses. Synaptic scaling is multiplicative, meaning that all synaptic weights are up- or down-modulated by the same scaling factor, and thus relative synaptic weights are preserved after up- or down-scaling (G. G. Turrigiano et al., 1998). Moreover, scaling regulates both AMPA and NMDA currents (Watt, van Rossum, MacLeod, Nelson, & Turrigiano, 2000). Thus, synaptic scaling has properties appropriate to stabilize neural firing while preserving synapse strengths. While synaptic scaling has predominantly been studied using activity manipulations in cell culture, multiple studies have documented similar plasticity mechanisms in response to sensory deprivation in vivo (Lambo & Turrigiano, 2013; Hengen, Lambo, Van Hooser, Katz, & Turrigiano, 2013; Keck et al., 2013). For example, visual deprivation initially drives a reduction in mean firing rate in mouse and rat visual cortex, which rapidly recovers via synaptic scaling back to pre-deprivation firing rate, even though deprivation continues (Hengen et al., 2013). Synaptic scaling restores firing rates over days, which is considerably slower than LTP and LTD. This suggests that while synaptic scaling may be an important mechanism for stabilizing mean firing rate, other, more rapid homeostatic mechanisms are also necessary to balance Hebbian plasticity (Zenke et al., 2013).

Another proposed mechanism for firing rate homeostasis is the sliding threshold model, or metaplasticity, in which a neuron dynamically adjusts its global threshold for induction of LTP or LTD (Bienenstock, Cooper, & Munro, 1982; Cooper & Bear, 2012). In this model, presynaptic firing rate is the critical parameter for determining whether LTD or LTP is induced at excitatory synapses, with firing rates below a 'synaptic modification threshold' driving LTD, and firing rates above that threshold driving LTP. The synaptic modification threshold is determined by recent activity, such that prolonged high activity increases the induction threshold to drive LTD across synapses. Conversely, a prolonged reduction in activity reduces the threshold to promote LTP. Like synaptic scaling, this mechanism controls firing rate through changes in synapse strength. Studies have found evidence for the sliding threshold model in sensory cortex, where sensory deprivation appears to lower the synaptic modification threshold to promote LTP (Guo et al., 2012; Kirkwood, Rioult, & Bear, 1996).

Firing rate homeostasis can also be mediated by plasticity of intrinsic excitability. Modulation of individual conductances strongly influences how a neuron responds to synaptic input. Early evidence for this form of plasticity came from studies of stomatogastric ganglion (STG) neurons from the spiny lobster, which fire in a rhythmic bursting pattern. This characteristic firing pattern acutely depends on release of inhibitory drive and is immediately abolished when STG neurons are separated from these inputs. Remarkably, chronic isolation of STG neurons restores the bursting pattern; this effect is reversed by driving STG neurons to fire with rhythmic current injection (G. Turrigiano, Abbott, & Marder, 1994). These findings suggest that the bursting phenotype is homeostatically regulated through changes in intrinsic conductances. Indeed, the transition to burst firing is accompanied by an increase in calcium currents and a decrease in potassium currents (G. Turrigiano, LeMasson, & Marder, 1995). Thus, the intrinsic properties of neurons can be actively regulated to maintain certain aspects of firing patterns.

Moreover, these findings demonstrate how multiple distinct mechanisms can support one cellular or circuit phenotype.

In rodent cortex, plasticity of excitatory neuron intrinsic excitability contributes to firing rate homeostasis. Similar to synaptic scaling, early evidence for this type of plasticity came from studies of cultured V1 neurons, where blocking spiking for 48 hours with TTX was found to increase intrinsic excitability and decrease spike threshold (Desai, Rutherford, & Turrigiano, 1999). Later studies in mouse V1 showed that prolonged sensory deprivation also drives a homeostatic increase in pyramidal cell intrinsic excitability. In binocular V1, 6-day monocular and binocular deprivation both increase the intrinsic excitability of L2/3 pyramidal neurons. This is caused by an increase in input resistance and a decrease in spike threshold (Lambo & Turrigiano, 2013). Plasticity of intrinsic excitability is more rapid in monocular V1, where 2-day monocular deprivation increases pyramidal cell intrinsic excitability (Maffei & Turrigiano, 2008). Recent work shows that artificial suppression of pyramidal cell activity in V1 drives changes in pyramidal neuron intrinsic excitability. Pharmacogenetic suppression of firing in layer L2/3 pyramidal cells during the critical period for ocular dominance plasticity drives both synaptic scaling and an increase in intrinsic excitability (Wen & Turrigiano, 2021). Interestingly, performing the same manipulation in adults evoked synaptic scaling but failed to induce changes in intrinsic excitability, suggesting that in V1, homeostatic changes in pyramidal cell intrinsic excitability are confined to juvenile ages. Plasticity of excitatory neuron intrinsic excitability is also observed in S1. In L2/3, brief deprivation of all but one whisker increases spike threshold in spared-column pyramidal cells (Barth, 2004). In rats, plasticity of excitatory neuron excitability is prominent in L5, where unilaterally trimming all whiskers for 1–5 weeks drives an increase in burst firing and an increase in dendritic HCN channel density (Breton & Stuart, 2009). Thus, changes in the intrinsic excitability of excitatory neurons contribute to firing homeostasis over days to weeks.

Recent work demonstrated that plasticity of inhibitory circuits can also mediate firing rate homeostasis. This mechanism is the research topic of this thesis. Studies in sensory cortex show that that inhibitory circuits are rapidly plastic in response to sensory deprivation (Kuhlman et al., 2013; Li, Gainey, Goldbeck, & Feldman, 2014; Resnik & Polley, 2017). In this plasticity, deprivation rapidly weakens the gain of inhibitory circuits, thus reducing inhibition in pyramidal cells. The direction of this plasticity is appropriate to restore mean pyramidal cell firing rate after sensory deprivation, and thus this is likely another mechanism that contributes to firing rate homeostasis. Theoretical work suggests that homeostatic mechanisms on the same time scale as Hebbian plasticity may be necessary for stable network function (Zenke et al., 2013). Unlike synaptic scaling, rapid disinhibition occurs within one day of sensory deprivation and thus may operate closer to the timescale of Hebbian plasticity mechanisms.

In **Chapter 2**, we seek to identify the cellular and synaptic mechanisms that underlie rapid inhibitory circuit plasticity in primary somatosensory cortex (S1). We show that 1-day whisker deprivation weakens inhibition in L2/3 through a rapid reduction in parvalbumin (PV) interneuron intrinsic excitability (Gainey, Aman, & Feldman, 2018). These L2/3 PV interneurons

are the major source of feedforward inhibition that regulates sensory responsiveness in L2/3 pyramidal neurons. Our findings suggest that inhibitory circuit plasticity mediates rapid homeostasis of pyramidal cell activity, whereas synaptic scaling and plasticity of intrinsic excitability of excitatory neurons are responsible for homeostasis over longer time scales.

Do the cellular mechanisms for homeostatic inhibitory circuit plasticity mechanisms change over different time scales? In **Chapter 3**, we address this question by investigating the time course of rapid plasticity in S1. We show that sensory deprivation triggers a succession of distinct responses in PV cell physiology over days. Together, these findings demonstrate that cortical circuits use multiple homeostatic processes, both in inhibitory networks and excitatory networks, to stabilize cortical activity over different time scales.

References

Barth, A. L. (2004). Alteration of Neuronal Firing Properties after In Vivo Experience in a FosGFP Transgenic Mouse. *Journal of Neuroscience*, *24*, 6466–6475.

Bienenstock, E., Cooper, L., & Munro, P. (1982). Theory for the development of neuron selectivity: Orientation specificity and binocular interaction in visual cortex. *The Journal of Neuroscience*, *2*, 32–48.

Breton, J.-D., & Stuart, G. J. (2009). Loss of sensory input increases the intrinsic excitability of layer 5 pyramidal neurons in rat barrel cortex: Sensory deprivation increases excitability of pyramidal neurons. *The Journal of Physiology*, *587*, 5107–5119.

Cooper, L. N., & Bear, M. F. (2012). The BCM theory of synapse modification at 30: Interaction of theory with experiment. *Nature Reviews Neuroscience*, *13*, 798–810.

Desai, N. S., Rutherford, L. C., & Turrigiano, G. G. (1999). Plasticity in the intrinsic excitability of cortical pyramidal neurons. *Nature Neuroscience*, *2*, 515–520.

Gainey, M. A., Aman, J. W., & Feldman, D. E. (2018). Rapid Disinhibition by Adjustment of PV Intrinsic Excitability during Whisker Map Plasticity in Mouse S1. *The Journal of Neuroscience*, *38*, 4749–4761.

Guo, Y., Huang, S., de Pasquale, R., McGehrin, K., Lee, H.-K., Zhao, K., & Kirkwood, A. (2012). Dark Exposure Extends the Integration Window for Spike-Timing-Dependent Plasticity. *Journal of Neuroscience*, *32*, 15027–15035.

Hengen, K. B., Lambo, M. E., Van Hooser, S. D., Katz, D. B., & Turrigiano, G. G. (2013). Firing rate homeostasis in visual cortex of freely behaving rodents. *Neuron*, *80*, 335–342.

Keck, T., Keller, G. B., Jacobsen, R. I., Eysel, U. T., Bonhoeffer, T., & Hübener, M. (2013). Synaptic Scaling and Homeostatic Plasticity in the Mouse Visual Cortex In Vivo. *Neuron*, *80*, 327–334.

Kirkwood, A., Rioult, M. G., & Bear, M. F. (1996). Experience-dependent modification of synaptic plasticity in visual cortex. *Nature*, *381*, 526–528.

Kuhlman, S. J., Olivas, N. D., Tring, E., Ikrar, T., Xu, X., & Trachtenberg, J. T. (2013). A disinhibitory microcircuit initiates critical-period plasticity in the visual cortex. *Nature*, *501*, 543–546.

Lambo, M. E., & Turrigiano, G. G. (2013). Synaptic and Intrinsic Homeostatic Mechanisms Cooperate to Increase L2/3 Pyramidal Neuron Excitability during a Late Phase of Critical Period Plasticity. *Journal of Neuroscience*, *33*, 8810–8819.

Li, L., Gainey, M. A., Goldbeck, J. E., & Feldman, D. E. (2014). Rapid homeostasis by disinhibition during whisker map plasticity. *Proceedings of the National Academy of Sciences*, *111*, 1616–1621.

Maffei, A., & Turrigiano, G. G. (2008). Multiple Modes of Network Homeostasis in Visual Cortical Layer 2/3. *Journal of Neuroscience*, *28*, 4377–4384.

Miller, K. D., & MacKay, D. J. C. (1994). The Role of Constraints in Hebbian Learning. *Neural Computation*, *6*, 100–126.

O'Brien, R. J., Kamboj, S., Ehlers, M. D., Rosen, K. R., Fischbach, G. D., & Huganir, R. L. (1998). Activity-Dependent Modulation of Synaptic AMPA Receptor Accumulation. *Neuron*, *21*, 1067–1078.

Pozo, K., & Goda, Y. (2010). Unraveling Mechanisms of Homeostatic Synaptic Plasticity. *Neuron*, *66*, 337–351.

Resnik, J., & Polley, D. B. (2017). Fast-spiking GABA circuit dynamics in the auditory cortex predict recovery of sensory processing following peripheral nerve damage. *ELife*, *6*, e21452.

Turrigiano, G., Abbott, L. F., & Marder, E. (1994). Activity-dependent changes in the intrinsic properties of cultured neurons. *Science (New York, N.Y.)*, *264*, 974–977.

Turrigiano, G. G., Leslie, K. R., Desai, N. S., Rutherford, L. C., & Nelson, S. B. (1998). Activity-dependent scaling of quantal amplitude in neocortical neurons. *Nature*, *391*, 892–896.

Turrigiano, G., LeMasson, G., & Marder, E. (1995). Selective regulation of current densities underlies spontaneous changes in the activity of cultured neurons. *The Journal of Neuroscience*, *15*, 3640–3652.

Turrigiano, Gina G. (2008). The Self-Tuning Neuron: Synaptic Scaling of Excitatory Synapses. *Cell*, *135*, 422–435.

Watt, A. J., van Rossum, M. C. W., MacLeod, K. M., Nelson, S. B., & Turrigiano, G. G. (2000). Activity Coregulates Quantal AMPA and NMDA Currents at Neocortical Synapses. *Neuron*, *26*, 659–670.

Wen, W., & Turrigiano, G. G. (2021). Developmental Regulation of Homeostatic Plasticity in Mouse Primary Visual Cortex. *The Journal of Neuroscience: The Official Journal of the Society for Neuroscience*, *41*, 9891–9905.

Zenke, F., Hennequin, G., & Gerstner, W. (2013). Synaptic Plasticity in Neural Networks Needs Homeostasis with a Fast Rate Detector. *PLoS Computational Biology*, *9*, e1003330.

Chapter 2

Rapid disinhibition by adjustment of PV intrinsic excitability during whisker map plasticity in mouse S1

Melanie A. Gainey, Joseph W. Aman & Daniel E. Feldman

This chapter, in full, is a republication of the material as it appears in Gainey, M. A., Aman, J. W., & Feldman, D. E. (2018). Rapid Disinhibition by Adjustment of PV Intrinsic Excitability during Whisker Map Plasticity in Mouse S1. The Journal of Neuroscience, 38(20), 4749–4761.

2.1 SUMMARY

Rapid plasticity of layer (L) 2/3 inhibitory circuits is an early step in sensory cortical map plasticity, but its cellular basis is unclear. We show that, in mice of either sex, 1 day whisker deprivation drives rapid loss of L4-evoked feedforward inhibition and more modest loss of feedforward excitation in L2/3 pyramidal (PYR) cells, increasing E-I conductance ratio. Rapid disinhibition was due to reduced L4-evoked spiking by L2/3 parvalbumin (PV) interneurons, caused by reduced PV intrinsic excitability. This included elevated PV spike threshold, associated with an increase in low-threshold, voltage activated delayed rectifier (presumed Kv1) and A-type potassium currents. Excitatory synaptic input and unitary inhibitory output of PV cells were unaffected. Functionally, the loss of feedforward inhibition and excitation were precisely coordinated in L2/3 PYR cells, so that peak feedforward synaptic depolarization remained stable. Thus, rapid plasticity of PV intrinsic excitability offsets early weakening of excitatory circuits to homeostatically stabilize synaptic potentials in PYR cells of sensory cortex.

Significance statement

Inhibitory circuits in cerebral cortex are highly plastic, but the cellular mechanisms and functional importance of this plasticity are incompletely understood. We show that brief (1-day) sensory deprivation rapidly weakens parvalbumin (PV) inhibitory circuits by reducing the intrinsic excitability of PV neurons. This involved a rapid increase in voltage-gated potassium conductances that control near-threshold spiking excitability. Functionally, the loss of PV-mediated feedforward inhibition in L2/3 pyramidal cells was precisely balanced with the separate loss of feedforward excitation, resulting in a net homeostatic stabilization of synaptic potentials. Thus, rapid plasticity of PV intrinsic excitability implements network-level homeostasis to stabilize synaptic potentials in sensory cortex.

2.2 INTRODUCTION

Parvalbumin (PV) inhibitory circuits are highly plastic to altered sensory experience, and contribute to receptive field plasticity in sensory cortex (Froemke, 2015). PV circuit plasticity is evident after just 1-2 d of visual or auditory deprivation or 3 d of whisker deprivation, and thus is an early step in cortical plasticity. In layer (L) 2/3, deprivation reduces PV-mediated inhibition, which can increase sensory-evoked responses in pyramidal (PYR) cells and enable subsequent Hebbian plasticity (Kuhlman et al., 2013; Li et al., 2014; Resnik and Polley, 2017) (Gambino and Holtmaat, 2012; Donato et al., 2013; Kuhlman et al., 2013; Froemke, 2015). Disinhibition may also implement rapid homeostasis to stabilize and maintain mean PYR firing rate for several days prior to the onset of ocular dominance or whisker map plasticity (Hengen et al., 2013; Li et al., 2014; Barnes et al., 2015; Gainey and Feldman, 2017; Turrigiano, 2017).

Despite its functional importance, the cellular mechanisms for rapid disinhibition are incompletely understood. Best studied are structural changes, including loss of inhibitory synapses and structural remodeling of GABAergic axons (Marik et al., 2010; Keck et al., 2011; Chen et al., 2012; van Versendaal et al., 2012; Chen and Nedivi, 2013). Deprivation can also functionally weaken excitatory input synapses and inhibitory output synapses of PV cells (Maffei et al., 2004; Jiao et al., 2006; House et al., 2011; Kuhlman et al., 2013; Xue et al., 2014; Sun et al., 2016). In contrast, whether experience alters intrinsic excitability of PV neurons has been less clear. Molecular pathways exist for activity-dependent regulation of PV intrinsic excitability, but whether experience engages these mechanisms to rapidly alter intrinsic excitability *in vivo* is unknown (Li et al., 2011; Dehorter et al., 2015). Mechanisms for PV circuit plasticity have been mostly studied after long-term activity manipulation (days or weeks) (Jiao et al., 2006; Sun, 2009; House et al., 2011; Kätzel et al., 2011; Xue et al., 2014), and thus, the mechanisms that underlie rapid disinhibition remain murky.

We examined the mechanisms for rapid disinhibition in L2/3 of somatosensory cortex (S1). In rats, 5-7 d of whisker deprivation reduces feedforward and recurrent inhibition in L2/3 PYR cells, mediated by weakening excitatory synapses onto PV neurons (House et al., 2011; Shao et

al., 2013). Disinhibition also occurs in rats after 3 d deprivation, where it is thought to homeostatically stabilize whisker-evoked firing in L2/3 PYR cells, but mechanisms for this rapid disinhibition are unknown (Li et al., 2014). Here, we examined rapid disinhibition after 1 d whisker deprivation in mice, which matches the briefest period of deprivation known to induce disinhibition in visual cortex (Kuhlman et al., 2013). 1 d deprivation robustly weakened feedforward L4-L2/3 inhibition in L2/3 PYR cells, due to reduced L2/3 PV neuron spiking. Unlike in prior studies of PV circuit plasticity, this was not due to reduced synaptic drive onto PV cells, but instead was caused by rapid reduction of PV intrinsic excitability. This was mediated by increased voltage-activated potassium currents that elevated PV spike threshold, reducing near-threshold excitability. Functionally, rapid disinhibition preserved net L4-evoked peak synaptic responses in L2/3 PYR cells, suggesting that rapid plasticity of PV intrinsic excitability acts to homeostatically stabilize sensory responses in the PYR network during ongoing changes in sensory use.

2.3 MATERIALS & METHODS

Procedures were approved by the UC Berkeley Animal Care and Use Committee and followed NIH guidelines. PV-IRES-Cre mice (Jackson #008069; https://www.jax.org/strain/008069) (Hippenmeyer et al., 2005) were crossed with Cre-dependent TdTomato reporter (Ai14) mice (Jackson #007914; https://www.jax.org/strain/007914) (Madisen et al., 2010) to generate PV-Cre;tdTomato offspring. Layer 4 optogenetics experiments were done in Scnn1a-Tg3-Cre mice (https://www.jax.org/strain/009613). Mice were housed as litters in standard cages. For whisker deprivation, the right D-row whiskers (D1-D6 and gamma) were plucked under transient isoflurane anesthesia, 24 ± 2 hr before slice preparation. Sham-plucked littermates underwent anesthesia but not plucking.

Slice Preparation

P18-P21 mice of either sex were anesthetized with isoflurane and decapitated. Brain slices were prepared using a Leica VT1200S vibratome in chilled oxygenated low-sodium, low-calcium Ringer's solution (in mM: 85 NaCl, 75 Sucrose, 25 D-(+)-glucose, 4 $MgSO_4$, 2.5 KCl, 1.25 Na_2HPO_4, 0.5 ascorbic acid, 25 $NaHCO_3$, and 0.5 $CaCl_2$, 320 mOsm). Cortical slices (350 µm) were cut from the left hemisphere in the "across-row" plane, oriented 50° toward coronal from the midsagittal plane and 35° degrees from vertical. Using this plane, each slice contains one column from each whisker row A-E, and within-column circuits are largely preserved (Finnerty et al., 1999; Allen et al., 2003). Slices were transferred to standard Ringer's solution (in mM: 119 NaCl, 26.2 $NaHCO_3$, 11 D-(+)-glucose, 1.3 $MgSO_4$, 2.5 KCl, 1 NaH_2PO_4, 2.5 $CaCl_2$, 300 mOsm) for 30 minutes at 30°C and then kept at room temperature until recording (0.5-7 hr).

Slice electrophysiology and L4-evoked synaptic responses

Recordings were made at 30-31°C in standard Ringer's solution. Barrel columns were identified by transillumination at 4x, and visually-guided patching was performed using infrared differential interference contrast optics at 40x. L2/3 PYR cells were identified by soma shape, and were located ~100-240 mm below the L1-L2 boundary, within ~100 mm tangentially of column center. PV neurons were identified by tdTomato fluorescence (530-550 nm bandpass excitation, 575-625 nm emission, Dage-MTI camera). PYR cell recordings were made in PV-Cre;tdTomato or C57BL/6 mice (https://www.jax.org/strain/000664).

All recordings were made in L2/3 of D-row barrel columns, with the NMDA receptor antagonist 50 µM D-AP5 in the bath. Whole-cell recording was performed with 3-5 MΩ pipettes using a Multiclamp 700B amplifier (Molecular Devices, Sunnyvale CA) with 2 kHz low-pass filtering and 7-10 kHz digitization. L4-evoked synaptic responses were elicited using 200-µs current pulses delivered via a bipolar stimulating electrode (115 µm tip spacing, FHC, Bowdoin, ME) placed in the center of the D barrel in L4. Interstimulus interval was 10 sec. For input-output curves, EPSC threshold (Eθ) was defined as the minimal stimulation current that evoked an EPSC in 5 consecutive sweeps. For L2/3 PYR cells, Eθ was determined individually for each cell. For PV cells, Eθ was defined as the average Eθ measured for two co-columnar L2/3 PYR cells.

Voltage clamp recordings of synaptic currents used cesium gluconate internal solution (in mM: 108 D-gluconic acid, 108 CsOH, 20 HEPES, 5 tetraethylammonium-Cl, 2.8 NaCl, 0.4 EGTA, 4 MgATP, 0.3 NaGTP, 5 BAPTA, 5 QX-314 bromide, pH 7.2, 295 mOsm). V_{hold} was corrected for the liquid junction potential (12 mV). Series resistance was monitored in each sweep and was compensated by 40-80%. Cells whose input resistance changed >30% throughout recording were excluded from analysis. PYR cells with V_{rest} >= -60 mV were discarded. L4-evoked EPSCs and IPSCs were separated by recording at V_{hold} = -68 mV and 0 mV, respectively, which correspond to E_{Cl} and E_{AMPA}. Currents were converted to conductances using standard methods (Wehr and Zador, 2003; House et al., 2011). Integrated synaptic conductance was quantified in a window 3-23 ms after the stimulus.

Current clamp recordings were made using K gluconate internal solution (mM: 116 K gluconate, 20 HEPES, 6 KCl, 2 NaCl, 0.5 EGTA, 4 MgATP, 0.3 NaGTP, 5 Na_2phosphocreatine, pH 7.2, 295 mOsm). Series resistance artifacts were corrected by bridge balance. In PV cells, postsynaptic potentials (PSPs) were measured from a baseline of -68 mV, the mean V_{rest} of L2/3 PV neurons. PSP amplitude was quantified in a 1.8 ms window at the peak. In PYR cells, we measured L4-evoked PSPs from V_{rest} or from an estimated synaptic V_m (V_{syn}) of -55 mV achieved by somatic current injection. For the latter case, because cells in current clamp are not spatially isopotential, we performed a separate calibration experiment to estimate the difference between somatic V_m (V_{soma}) and V_{syn} during somatic current injection in these conditions. To do this, we recorded using modified K gluconate internal with Nernst potential for chloride of -50 mV, and found that somatic depolarization to -44.3 ± 1.3 mV was necessary to reverse pharmacologically isolated GABA-A mediated IPSPs in current clamp (n=4 cells). Thus, during

somatic current injection, V_{soma} was ~5 mV more depolarized than V_{syn}. Thus, in the main experiments, we depolarized V_{soma} to -50 mV to achieve an estimated V_{syn} of -55 mV.

Juxtacellular (loose-seal) recordings in PV cells were made using K gluconate internal. Spikes were detected in voltage-clamp mode with V_{hold} continuously adjusted to maintain 0 pA holding current. Spike probability was calculated over 10 sweeps for each L4 stimulus intensity.

Spontaneous miniature inhibitory postsynaptic currents (mIPSCs) were recorded in voltage clamp at V_{hold} = 0 mV, and isolated using 50 µM D-AP5, 10 µM NBQX, and 100 µM saclofen, and 0.1 µM TTX in the bath. Rseries compensation was not used for mIPSC recordings. Analysis was performed by semi-automatic template matching in Axograph X (Axograph Scientific, Sydney, Australia). Detection threshold was 5 pA. A minimum of 300 events were analyzed per cell. mIPSC analysis was done blind to experimental condition.

L4 optogenetic stimulation

Scnn1a-Cre mice were injected at P2-3 with AAV2.9-CAGGS-Flex-ChR2-tdTom-WPRE-SV40 virus into S1 (UPenn Vector Core, #V1345). Scnn1a-Cre mice express Cre in L4 excitatory cells (Adesnik and Scanziani, 2010; Madisen et al., 2010), and we verified L4 expression using AAV2.9-CAGGS-flex-tdTomato viral reporter (UPenn Vector Core, #V1682, not shown). Slices were prepared at P18-22. The D column was readily identifiable by L4 fluorescence, which revealed the barrel pattern. A 443-nm laser (40 mW, CrystaLaser DL445-040) was connected via optic fiber to the microscope epifluorescence arm and projected through a 4x objective to form a 238 µm diameter spot. This was centered over the D barrel in L4. Laser power at the slice was calibrated using a power meter (Newport 1916-R). We patched L2/3 PYR cells in the D column and synaptic responses were measured in voltage clamp (as above, except that Rseries was not compensated). 2-ms light pulses were applied at a 10-s interstimulus interval to activate L4 neurons and elicit synaptic responses in L2/3 PYR cells in the D column. For optogenetic input-output curves, Eθ was defined as the minimal laser power that evoked an EPSC in at least 5 of 10 consecutive sweeps, and was determined individually for each PYR cell. Other experimental parameters were identical to the L4 electrical stimulation experiments.
To ensure sufficient ChR2 expression level in each slice, we required that tdTomato fluorescence in L4 surpass a minimum brightness (200 intensity units), measured in a 350-um diameter circular region centered on the L4 D barrel, using identical excitation power and camera settings each day. We also quantitatively measured functional ChR2 expression level in L4 using the "photo-LFP" (Shao et al., 2013). For this measure, a 1.8–2.2 MΩ field potential pipette was placed in the center of the D barrel in L4 at the end of each slice recording, and TTX (1 µM) and kynurenic acid (2 mM) were added to the bath. Local field potential (LFP) evoked by L4 photostimulation at 1.6 x Eθ was measured, which reflects bulk photocurrent in the L4 neuron population. Photo-LFP magnitude correlated with tdTomato fluorescence (not shown). To ensure equivalent magnitude of presynaptic stimulation between Sham and Deprived groups, we restricted analysis to slices with L4 photo-LFP magnitude > 0.6 mV and < 0.25 mV.

Overall, 34/49 slices from 18/24 mice passed brightness and photo-LFP criteria, and were used for recordings.

PV-PYR cell pairs

To study unitary synaptic connections, we made dual whole-cell recordings from co-columnar PV and PYR neurons (< 60 mm apart). The PV cell was recorded in current clamp using K gluconate internal, and the PYR cell was recorded in voltage clamp using Cs gluconate internal. A 5-spike train was evoked in the PV cell using current pulses (2 ms, 1-2 nA, 50 ms interval). uIPSCs were recorded in the PYR cell at 0 mV. Approximately 30 sweeps were collected. uIPSC amplitude was calculated in a 1.8 ms window centered on the peak. IPSCs were scored as outward currents greater than 1 s.d. above spontaneous Vm, initiating within 3.6 ms of a presynaptic spike. Two cells were considered connected if the probability of observing an IPSC was significantly greater after the 1st PV spike than during spontaneous activity before the spike (assessed over 30 sweeps, α=0.05, binomial test). Paired pulse ratio was defined as 2nd uIPSC / 1st uIPSC amplitude. CV was calculated from variance of the 1st uIPSC – variance of a spontaneous epoch. uIPSC decay time constant (τ) was calculated from a single exponential fit.

PV intrinsic excitability

PV cells were recorded in whole-cell current clamp mode. Vrest was measured immediately after break-in. Series resistance artifacts were compensated by bridge balance. Input resistance was calculated as the slope of the linear fit of steady-state ΔVm during -50, 0, and +50 pA current steps. The membrane time constant (τ) was calculated by single exponential fit of the first 80 ms of the -50 pA current step. Rheobase was defined as the minimum current injection (500 ms) that elicited >=1 spike on 5 consecutive sweeps. The firing – current (F-I) relationship was measured using increasing currents above rheobase. F-I curve slope was measured from linear fit. Spike threshold was defined as the Vm at which the second derivative of Vm was > 6 s.d. above the pre-stimulus period. Spike latency was defined as time to spike threshold. Spike shape was analyzed for the 2nd-6th spikes during each current injection, excluding the 1st spike which has systematically different threshold in L2/3 PV cells (Goldberg et al., 2008). Cells with spike threshold > -20 mV, indicative of an under-compensated bridge, were excluded from analysis.

Potassium currents in PV neurons

Voltage-sensitive potassium (Kv) currents were recorded in voltage clamp, using K gluconate internal. To minimize calcium-gated K currents, the internal contained 5 mM BAPTA, and the Ringers contained low $CaCl_2$ (0.5 mM). Sweeps were collected at 2.5 s interval. To measure delayed rectifier K currents, the bath contained the synaptic blockers 50 µM D-AP5, 10 µM NBQX, 100 µM saclofen, and 3 µM SR 95531 hydrobromide (gabazine); the sodium channel blocker 0.1 µM TTX; the I_M blocker 10 µM XE 991 dihydrochloride; the I_h blocker 0.1 mM ZD2788; and 0.1% bovine serum albumin. After a prepulse to -70 mV, we applied 300-ms

voltage steps every 10 mV (-70 to -10 mV) and every 5 mV (-100 to -80 mV). Leak currents were measured from the second series, extrapolated to the first series, and subtracted. Delayed rectifier currents were identified as non-inactivating outward currents that activate at ~ -40 to -50 mV (Kv1 family) or -20 to -30 mV (Kv2 family). Current amplitude was measured in the last 100 ms of the 300-ms pulse. Inactivating (A-type) currents are also present in these recordings but inactivate in <50 ms, and were ignored in analysis (Coetzee et al., 1999). To separate Kv1.1 from other delayed rectifier currents, dendrotoxin-K (100 nM) was washed in, and DTX-insensitive currents were subtracted from the baseline current.

To measure I_A, we used a combination of pharmacology and inactivation properties. The bath contained the synaptic blockers 50 µM D-AP5, 10 µM NBQX, 100 µM saclofen, 3 µM SR 95531 hydrobromide (gabazine); 0.1 µM TTX; and 20 mM TEA to block most delayed rectifier current and I_M. A 200-ms prepulse to -70 mV was applied, and then Vm was stepped to 0 mV for 300 ms. In interleaved sweeps, the prepulse was changed to -40 mV, which inactivates I_A. We isolated I_A during the 0 mV step by subtracting sweeps with the -40 mV prepulse from sweeps with the -70 mV prepulse. Cells were held at -100 mV for 2.5 sec between sweeps, to allow recovery from inactivation. Current magnitude was quanitifed as integrated current from 1-26 ms after onset of the 0 mV step. A small amount of non-inactivating current was also observed after subtraction, and likely reflects I_h, which was not blocked in these experiments. We only analyzed the inactivating (I_A) component. Because I_A amplitude correlated with Rseries, cells were only included if residual Rseries was 5.5-10.5 Mohm, which allowed precise matching of Rseries between Sham and Deprived cell populations (7.6 ± 0.3 MW and 7.5 ± 0.3 MW, respectively, n = 16 cells per group).

Drugs

Drugs were from Tocris Biosciences (Ellisville, MO), except tetrodotoxin (TTX) and dendrotoxin-k, both from Alomone Labs (Jerusalem, Israel).

Parallel conductance model of PYR synaptic potentials

We used a standard parallel conductance model (Wehr and Zador, 2003) to predict synaptic potentials that would be generated in L2/3 PYR cells from recorded L4-evoked synaptic conductances. The model simulated synaptically evoked changes in Vm (ΔVm) resulting from L4-evoked excitatory and inhibitory conductance waveforms (Gex and Gin), recorded at 1.4x E threshold in a single PYR neuron. Gex and Gin waveforms were constrained to be non-negative and were smoothed (Savitzky-Golay, 1-ms window). ΔVm was predicted using the parallel conductance equation:

$$1)C\,(dV/dt) = G_{ex}(V_m-E_{ex}) + G_{in}(V_m-E_{in}) + G_{rest}(V_m-E_{rest})$$

C was 240 pF, which was the average membrane capacitance measured in PYR neurons in our study. G_{rest} was defined as 1 / R_{input}, where R_{input} was the average input resistance measured for

deprived cells (94 MW) or sham cells (100 MW). We simulated ΔV_m for cells at E_{rest} = -55 mV, in order to estimate the effect of feedforward synaptic input on V_m as a cell approaches spike threshold. V_m was calculated by integrating Eθ. 1 from a starting value of V_m=-55 mV with 0.1 ms time resolution, using Euler's method. This is the same method used in (House et al., 2011).

Experimental Design and Statistical Analysis

D-row deprived and sham mice were littermates, and were either recorded interleaved on the same day or on alternate days. All reported deprivation effects were observed across at least 3 independent litters. For each measurement type, data were tested for Gaussian distribution prior to use of parametric statistics. Non-Gaussian data were evaluated using either log-transformed data, non-parametric statistics or by permutation test, as indicated in the text. Reported values are mean ± SEM, except where indicated. All statistical tests are identified in the Results text. Statistical analysis was performed in Matlab, Excel or R.

2.4 RESULTS

To test whether brief, 1 day whisker deprivation drives inhibitory circuit plasticity in L2/3 of S1, we plucked the right-side D-row whiskers in mice at P17-20, 24 hrs prior to slice preparation at P18-21. We cut S1 slices in the "across-row" plane that allows D whisker columns to be visually identified by transillumination (Finnerty et al., 1999; Allen et al., 2003) (**Fig. 1A**, top). We used multiple approaches to compare cell and circuit physiology in L2/3 of the D column between 1-day D-row deprived mice and age-matched, sham-deprived littermates. Most experiments used PV-Cre;tdTomato mice to enable fluorescence-guided recording from L2/3 PV neurons.

Stimulation near Eθ typically elicited an EPSC and a small IPSC. Stronger stimulation recruited larger currents, with inhibition dominating over excitation by 1.2-1.4 x Eθ (**Fig. 1B**), similar to rats (House et al., 2011; Shao et al., 2013). NBQX (10 mM) blocked 85 ± 3.6% of the L4-evoked IPSC at 1.4 x Eθ (**Fig. 1C**; n = 6 cells, 5 mice), and the latency of the NBQX-sensitive IPSC was 1.05 ± 0.26 ms longer than the EPSC in the same cell. These properties indicate that ~ 85% of the measured IPSC was feedforward, disynaptic inhibition, and that contamination by monosynaptic inhibition was modest. For analysis, EPSCs and IPSCs were converted to conductances (Gex and Gin) using standard methods (Wehr and Zador, 2003; House et al., 2011).

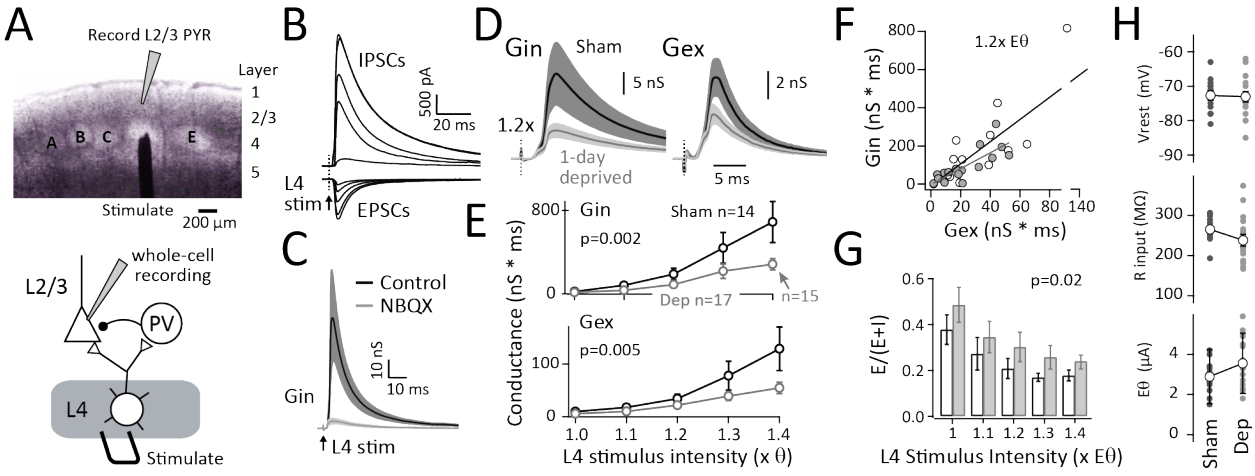

Figure 1. 1-day deprivation weakens L4-evoked inhibition and increases E-I conductance ratio in L2/3 PYR cells. **A,** Top: S1 slice with stimulating electrode in L4 of D barrel, and schematic recording electrode. Bottom: Circuit for L4-L2/3 feedforward excitation and inhibition. **B,** L4-evoked IPSCs and EPSCs in an example L2/3 PYR cell. Increasing currents are responses to L4 stimulation at 1.0-1.4x Eθ. **C**, Mean L4-evoked Gin at 1.4x Eθ before and after NBQX application (n=6 cells). Shading is SEM. **D,** Mean L4-evoked Gin and Gex waveforms at 1.2x Eθ across all sham (n=14) and deprived (n=17) cells. Shading is SEM. **E,** Input-output curves for integrated Gin and Gex with increasing L4-stimulation intensity. Points are mean ± SEM. Two deprived cells showed unclamped action currents at 1.4x Eθ at Vhold = 0 mV, and were therefore omitted from Gin analysis at 1.4x Eθ. p-values are for sham vs. deprived factor in 2-way ANOVA. **F,** Left: Within-cell comparison of Gex vs Gin at 1.2x Eθ. Each point is a cell. Lines are linear regression for sham (black) and deprived (gray). **G,** E-I conductance ratio, quantified as Gex / (Gex + Gin), across stimulus intensities. Bars shown mean ± SEM, as in all subsequent figures. P-value is sham vs. deprived factor in 2-way ANOVA. **H,** V_{rest}, R_{input} and Eθ for each cell (dots) and population mean (open circle).

1 d whisker deprivation reduced input-output curves for both L4-evoked Gex and Gin in L2/3 PYR cells (Sham: n = 14 cells, 11 mice; Dep: n = 17 cells, 12 mice; Gex: $F(1,4)=8.44$, $p=0.0043$; Gin: $F(1,4)=11.2$, $p=0.001$; 2-factor ANOVA) (**Fig. 1D-E**). At 1.2 x Eθ, mean integrated excitation was reduced by 36%, and inhibition was reduced by 53%. Gex and Gin were correlated within individual cells (linear fit, $R^2=0.79$) (Xue et al., 2014), and deprivation reduced the slope of this relationship, suggesting preferential loss of Gin (**Fig. 1F**). We calculated E-I conductance ratio as E/(E+I) for each cell, and found a significant increase in E/(E+I) for deprived cells across stimulus intensities ($F(1,4)=5.88$, $p=0.017$) (**Fig. 1G**). V_{rest}, R_{input} and Eθ were not altered by deprivation, indicating that recording quality and stimulation efficacy were equal in sham vs. deprived groups (**Fig. 1H**). Thus, 1 day deprivation reduced both Gin and Gex, as previously reported for 5+ day deprivation in rats (Shepherd et al., 2003; House et al., 2011; Shao et al., 2013), and Gin was preferentially weakened to elevate E-I conductance ratio. This inhibitory plasticity is the most rapid yet reported in S1 cortex.

Optogenetic activation of the feedforward L4-L2/3 circuit

To confirm that deprivation affected the L4-L2/3 projection specifically, we assayed L4-L2/3 circuits optogenetically. We expressed ChR2-tdTomato in L4 excitatory cells in S1 using a Cre dependent viral vector in Scnn1a-Tg3-Cre mice, which express Cre in L4 excitatory cells (Adesnik and Scanziani, 2010; Madisen et al., 2010) (**Fig. 2A**). D-row whiskers were deprived or sham-deprived at P17-21, and slices were made 24 hrs later. We activated L4 neurons using a calibrated blue laser spot centered in the D barrel in L4, and recorded postsynaptic currents from a L2/3 PYR cell in the D column in voltage clamp (**Fig. 2B**). We determined Eθ as the minimal laser intensity that evoked a reliable EPSC in the L2/3 PYR cell, and measured input-output curves for EPSCs and IPSCs at 1.0-2.0 x Eθ. Near Eθ, photostimulation evoked small EPSCs and IPSCs. Increasing photostimulus intensity recruited larger EPSCs and IPSCs, with IPSCs increasing preferentially to dominate the response (**Fig. 2C**). This result is similar to L4 electrical stimulation (**Fig. 1**) and to optogenetic activation of L2/3 recurrent networks in slice and *in vivo* (Mateo et al., 2011; Shao et al., 2013). Evoked currents were somewhat smaller and slower than with electrical stimulation. Evoked IPSCs were completely blocked by the glutamate receptor antagonist kynurenic acid (2 mM), with no contamination by monosynaptic inhibition (**Fig. 2D**).

1-day deprivation reduced input-output curves for both photo-evoked Gex and Gin (n=21 Sham and 26 Deprived cells; Gex: $F(1,5)=13.4$, $p=0.0003$; Gin: $F(1,5)=12.3$, $p=0.00054$; 2-factor ANOVA on log-transformed data, **Fig. 2E**). Deprivation reduced Gex and Gin waveforms but kinetics were unaffected. Deprivation also increased E-I ratio, calculated as E/(E+I) within each cell ($F(1,5)=11.1$, $p=0.00096$; **Fig. 2F**). This was particularly apparent at low photostimulus intensities, representing initial recruitment of the feedforward circuit. There was no difference between Sham and Deprived groups in photo-LFP magnitude in L4, which reflects bulk ChR2 photocurrent (see Methods), size of the EPSC at Eθ or laser power at Eθ (t-test, $p=0.16$, $p=0.47$, 0.96). These results indicate similar presynaptic L4 activation and initial recruitment of L4-L2/3 excitation in the two conditions (**Fig. 2G**). Thus, deprivation weakens feedforward L4-L2/3 excitation and inhibition, measured selectively by L4 optogenetic stimulation.

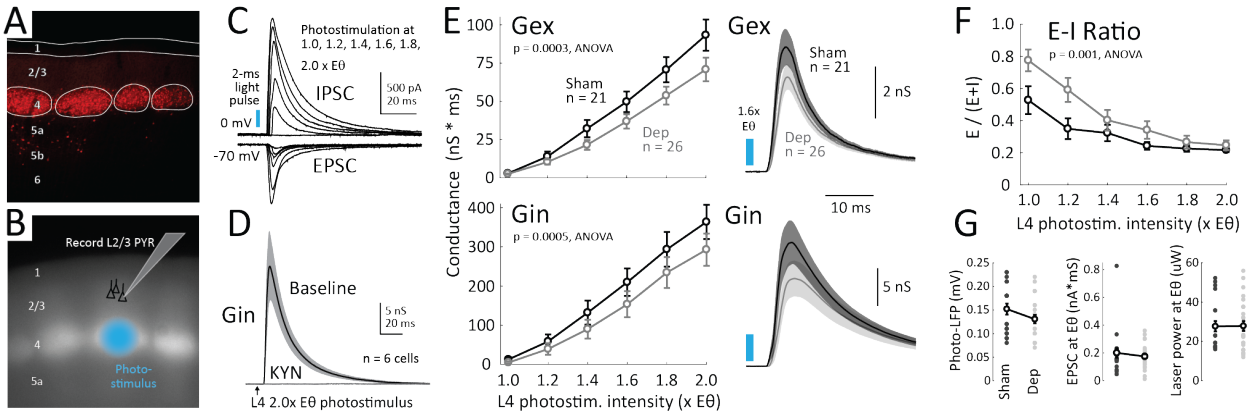

Figure 2. Optogenetically evoked L4-L2/3 excitatory and inhibitory conductances in L2/3 PYR cells are reduced by deprivation. A, Histological section of S1 from Scnn1a-Tg3-cre mouse injected with AAV2.9-CAGGS-flex-tdTom. tdTomato signal (red) is restricted to L4, except for a few L5 neurons. White outlines are L4 barrels. **B,** Live fluorescence image during a physiology experiment of slice from a mouse injected with flex-ChR2-tdTom virus. Bright signal is ChR2-tdTomato in L4 soma and axons. Schematic shows photostimulation spot in L4 and whole-cell recording in L2/3 of the D column. **C,** Photo-evoked IPSCs and EPSCs in an example L2/3 PYR cell. Increasing currents are responses to L4 optogenetic stimulation at 1.0-2.0x Eθ. **D,** Mean IPSC (n=6 cells) is completely blocked by bath application of kynurenic acid. **E,** Left, Mean input-output curves for L4-evoked Gex and Gin with increasing photostimulus intensity. Points are mean ± SEM. p-values are for Sham vs. Deprived factor in 2-factor ANOVA on log-transformed data. Right, Mean conductance waveforms at 1.6x Eθ. **F,** E-I conductance ratio across stimulation intensities, quantified as Gex / (Gex + Gin). **G,** Sham and Deprived groups did not differ in photo-LFP amplitude (measured in L4 at 1.6x Eθ), EPSC at Eθ, or laser power at Eθ. Each dot is a cell, open circles are population mean ± SEM.

Gex and Gin magnitude, kinetics, and input-output curve shape differed moderately between electrical and ChR2 stimulation experiments (**Figs. 1D-G and 2E-F**). This likely reflects differences in cellular specificity, spike synchrony and spatial focus of the two methods, and the use of Rseries compensation in the electrical but not optogenetics experiment. Deprivation produced nearly identical physiological effects despite these methodological differences.

L4-evoked spiking in L2/3 PV cells

To identify the circuit mechanism underlying weakened L4-L2/3 feedforward inhibition, we studied L2/3 PV interneurons, which classically mediate this inhibition (Helmstaedter et al., 2008; House et al., 2011; Xue et al., 2014). We first tested whether deprivation alters L4-evoked spiking of L2/3 PV cells. We recorded in the D column of PV-Cre;tdTomato mice (**Fig. 3A-B**). In each column, we determined mean Eθ in two PYR cells, and then recorded L4-evoked spikes in L2/3 PV cells in cell-attached mode, in response to L4 electrical stimulation at multiples of Eθ. In sham mice, a small number of PV spikes occurred at < 1.4 x Eθ, and most PV spiking occurred from 1.8-2.2 x Eθ (n=28 PV cells, 7 mice, **Fig. 3C**). L2/3 PYR cells recorded in cell-attached mode did not spike at all in this stimulus range (n=24 cells, 6 mice). 1-day D-row deprivation strongly reduced spike probability in PV cells (n=19 cells, 6 mice, **Fig. 3C**) as well as the fraction of PV cells spiking to each stimulus (**Fig. 3D**). Deprivation reduced mean spike probability by 63%, from 0.49 ± 0.07 spikes/stimulus in sham cells

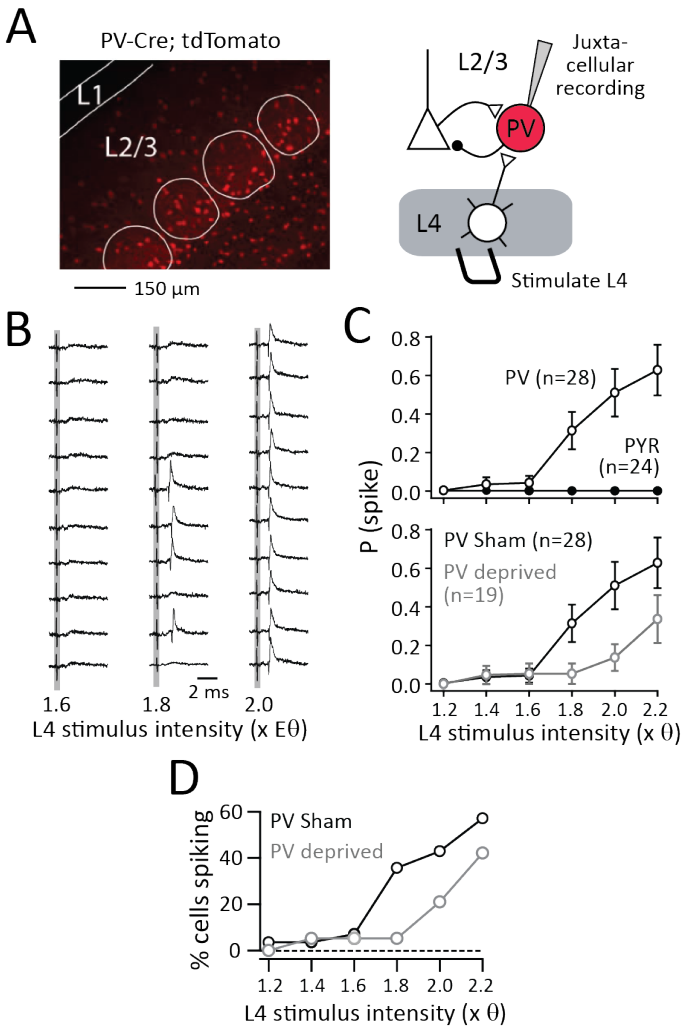

Figure 3. Deprivation reduces L4-evoked spiking of L2/3 PV cells. A, Left: Fluorescent PV cells in S1 slice from PV-Cre/TdTomato mouse. White, L4 barrels. Right, Schematic of cell-attached recording of L4-evoked spikes in L2/3 PV neurons. **B,** Example spiking data from one PV neuron. 10 sweeps at 3 stimulation intensities are shown. Gray, stimulus artifact. **C**, Mean spike probability for PV and PYR neurons from sham mice (top), and for PV neurons in sham vs. deprived mice (bottom). D, Fraction of PV cells spiking in sham vs. deprived mice.

(combined across 1.8-2.2x Eθ) to 0.18 ± 0.05 in deprived cells. This decrease was significant (p=0.034, permutation test on summed spikes across the input-output curve). Deprivation did not alter latency of evoked spikes (at 2.2x: Sham, 5.71 ± 0.52 ms; Deprived: 5.23 ± 0.42 ms). The rapid loss of feedforward inhibition in L2/3 PYR cells is therefore mediated, at least in part, by reduced L4-evoked spiking in PV neurons, as occurs with brief deprivation in visual cortex (Kuhlman et al., 2013).

Synaptic input to L2/3 PV cells

Prolonged (6-12 day) whisker deprivation in rat S1 and brief (1-day) visual deprivation in mouse V1 both reduce spiking of L2/3 PV cells by weakening L4 excitatory synaptic drive onto PV cells (House et al., 2011; Kuhlman et al., 2013; Sun et al., 2016). To test whether the same mechanism is engaged during 1-day whisker deprivation in mice, we made whole-cell voltage-clamp recordings from L2/3 PV cells in PV-Cre;tdTomato mice. We measured input-output curves for L4 electrical stimulation-evoked Gex and Gin in PV cells at 1.0-2.2x Eθ, where Eθ was determined as the mean Eθ for two co-columnar PYR cells. Surprisingly, L4-evoked Gex was

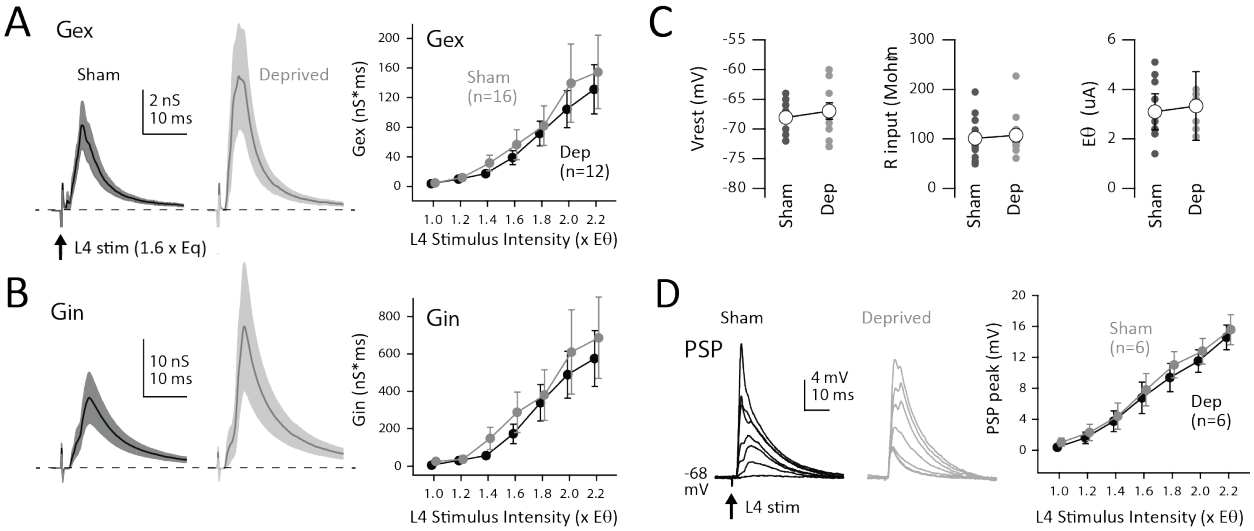

Figure 4. L4-evoked synaptic input to L2/3 PV cells remains normal during deprivation. A, Mean L4-evoked excitatory synaptic conductance in sham and deprived mice. Left, mean Gex waveform at 1.6x stimulation intensity. Right, mean integrated Gex across stimulus intensities. Shaded regions and bars are SEM. **B,** Mean L4-evoked inhibitory synaptic conductance. Conventions as in (A). Curves are displaced slightly along the x-axis for readability. **C,** Vrest, Rinput and Eθ for L2/3 PV cells in the experiments in (A, B). **D**, Left, L4-evoked PSPs in two example PV cells at 1.0, 1.2, ..., 2.2x Eθ. Right, Mean PSP peak above -68 mV baseline Vm, for all PV cells in sham vs. deprived mice. One cell in each group spiked beginning at 1.8 x Eθ

identical between sham and deprived cells (sham: n = 16 cells, 10 mice; deprived: n = 12 cells, 8 mice; F(1,6)=1.5, p = 0.22, 2-factor ANOVA), as was Gin (also F(1,6)=1.5, p = 0.22) (**Fig. 4A-B**). Vrest, Rinput and Eθ were unchanged between sham and deprived PV cells (**Fig. 4C**), as were Rseries and whole-cell capacitance (not shown). We also performed separate recordings from PV cells in current clamp, and measured input-output curves for L4-evoked postsynaptic potentials (PSPs). Baseline Vm was held at -68 mV in this experiment, which is equal to mean Vrest for L2/3 PV cells (**Fig. 4C**). The L4-evoked PSP peak was identical between sham and deprived mice (sham: n= 6 cells, 3 mice; deprived: n = 6 cells, 4 mice; F(1,6)=1.53, p=0.22, ANOVA) (**Fig. 4D**). Thus, multiple measures of synaptic input to PV cells revealed apparently normal synaptic input after 1 day deprivation, suggesting that PV spiking is reduced by a different mechanism than for prolonged whisker deprivation.

L2/3 PV inhibition onto L2/3 PYR cells

Weakening of feedforward inhibition in L2/3 PYR cells could also reflect weakening or loss of inhibitory synapses on L2/3 PYR cells, as occurs after long-duration activity manipulations (Xue et al., 2014). To test this, we first examined whether 1-day deprivation weakens unitary IPSCs (uIPSCs) from L2/3 PV to PYR cells. We made dual whole-cell recordings from nearby L2/3 PV and PYR cells in D whisker columns (**Fig. 5A**). We recorded uIPSCs in the PYR cell (in voltage clamp with Cs internal at 0 mV Vhold) in response to a 5-spike train in the PV cell (**Fig. 5B**). uIPSC amplitude was not decreased in deprived slices. Indeed, deprived pairs showed a non-

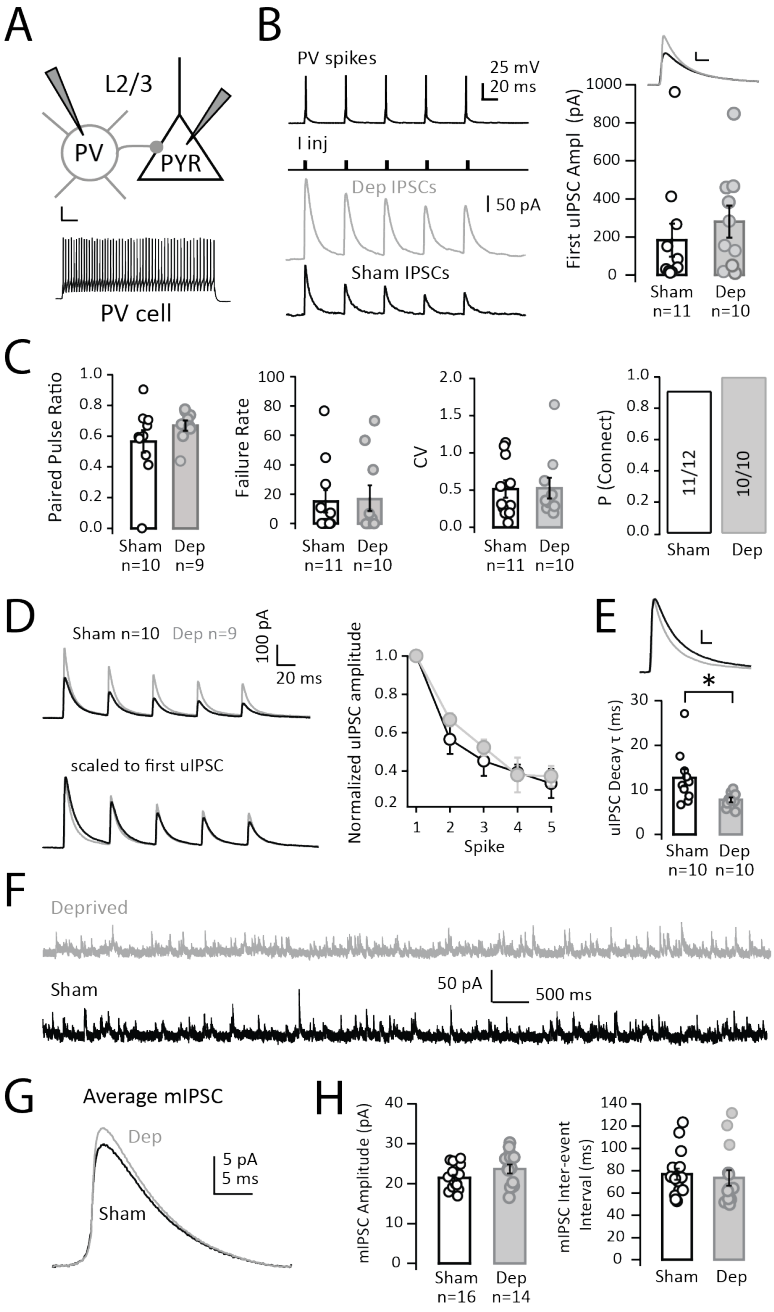

Figure 5. unitary PV→PYR IPSCs and mIPSCs on L2/3 PYR cells. A, Schematic for PV→PYR paired recordings. Bottom, example presynaptic PV spike train. Scale bar is 20 mV, 50 ms. **B**, Left, Presynaptic PV spike train and example uIPSCs evoked in one deprived and one sham PYR cell. I_{inj}, current injection to evoke presynaptic spikes. Right, Mean uIPSC1 waveform and amplitude for all Sham and Deprived pairs. Each dot is one pair. **C**, Paired pulse ratio (uIPSC2/uIPSC1), uIPSC1 failure rate, uIPSC1 coefficient of variation (CV), and probability of connected pairs. Each dot is one pair. **D**, Left: Population mean uIPSC train for Sham and Deprived pairs (top), normalized to first uIPSC peak (bottom). Deprived pairs showed no evidence of uIPSC weakening, and a non-significant trend toward uIPSC strengthening, with no change in short-term plasticity during the train (right). **E**, Mean uIPSC1 across all cells, and analysis of decay τ. Each dot is one pair. **F,** Example mIPCSs recorded at 0 mV in one Sham and one Deprived L2/3 PYR cell. **G**, Mean mIPSC waveform (n=16 Sham, n=14 Deprived cells). **H**, mIPSC amplitude and inter-event interval (IEI) for sham and deprived cells. Each circle is one cell.

significant trend for a larger first uIPSC (uIPSC1) (sham: n=11 pairs, 9 mice, 183 ± 87 pA ; deprived n= 10 pairs, 8 mice, amplitude: 280 ± 84 pA; t(19)=-0.80, p= 0.43, t-test) (**Fig. 5B**). This was not due to variation in inter-soma distance (sham: 24.2 ± 5.1 µm, deprived: 35.4 ± 4.6 µm, n.s., t(18)=-1.58, p=0.13, t-test). Deprivation did not alter paired-pulse ratio (uIPSC2/uIPSC1), failure rate for uIPSC1, coefficient of variation (CV) for uIPSC1, or connection probability (**Fig. 5C**). Deprivation did not alter short-term depression during the 5-spike train (**Fig. 5D**). Deprivation did speed the decay kinetics of uIPSC1 (decay τ in sham: 12.8 ± 1.9 ms; deprived: 7.8 ± 0.5 ms; t(18)=2.54, p = 0.02, t-test), which could suggest changes in GABA receptor

subunit composition or other modification of gating properties with deprivation (Fritschy and Panzanelli, 2014) (**Fig. 5E**).

To screen more broadly for weakening of inhibitory synapses on PYR cells, we analyzed spontaneous miniature IPSCs (mIPSCs) in L2/3 PYR cells in the D column (**Fig. 5F**). Deprivation did not weaken mIPSCs. Instead we observed a non-significant trend towards larger mIPSCs (sham: 21.5 ± 0.75 pA amplitude, n=16 cells, 3 mice; deprived 23.7 ± 0.1 pA, n=14 cells, 3 mice; t(28)=-1.69, p = 0.10, t-test), and no change in inter-event interval (IEI) (sham: 77.0 ± 5.0 ms, IEI: 73.6 ± 7.0 ms; t(28)=0.40, p = 0.69). Thus, we found no evidence for weakened inhibitory synapses onto L2/3 PYR cells after 1 d deprivation, either from mIPSCs or PV->PYR uIPSCs. If anything, small trends were apparent towards increased uIPSCs and increased mIPSC amplitude, reminiscent of the strengthening of PV->PYR uIPSCs after 5+ days deprivation in rats (House et al., 2011).

Reduced intrinsic excitability of L2/3 PVs cells

Could the reduction in L4-evoked PV spiking reflect reduced intrinsic excitability of PV cells? PV intrinsic excitability is plastic in response to extensive pharmacological or genetic blockade of network activity (Miller et al., 2011; Dehorter et al., 2015), and to 30-day whisker deprivation (Sun, 2009). To test whether 1-d deprivation alters intrinsic excitability, we made current clamp recordings from L2/3 PV cells in the presence of synaptic blockers (in µM: 50 D-AP5, 10 NBQX, 3 gabazine), and injected 500-ms current steps to evoke spikes and measure frequency-current (F-I) curves (**Fig. 6A**). Deprivation reduced PV spiking, causing a 22% reduction in the slope of F-I curves (n = 24 sham cells, 23 deprived cells; F(1,6)=12.6, p = 0.0004, 2-factor ANOVA). This corresponded to a reduction from 31.2 ± 2.1 to 25.0 ± 2.1 spikes at 80 pA above rheobase (**Fig. 6B**). This was associated with depolarized spike threshold (Sham: -35.3 ± 0.05 mV, n=7626 spikes; Dep: -32.3 ± 0.05 mV, n=6123 spikes, p = 1e-5, t-test, calculated for all spikes at 0-40 pA above rheobase) (**Figure 6C**). In contrast, Vrest, membrane time constant, input resistance and rheobase were unchanged (**Figure 6D**). Analysis of spike shape showed that deprivation increased mean spike threshold by 2.6 mV and decreased spike height (peak-threshold) (54.2 ± 1.3 vs. 50.0 ± 1.6 mV, t(44)=2.08, p=0.04, t-test), but did not alter peak Vm, spike width or afterhyperpolarization (p=0.34, p=0.13, p=0.49) (**Figure 6E-F**).

Many L2/3 PV cells exhibit a delayed spiking phenotype characterized by a long first-spike latency at rheobase (Gibson et al., 1999; Goldberg et al., 2008), which we also observed (**Figure 6G**). Prolonged up- or down-modulation of network activity can alter first-spike latency due to plasticity of voltage-activated potassium currents (Goldberg et al., 2008; Dehorter et al., 2015). We found that 1-day deprivation increased first spike latency by ~20 ms (F(1,6)=9.6, p=0.0021, 2-factor ANOVA) (**Fig 6H-I**), which lowered spike probability in early time windows after current injection onset (F(1,9)=11.2, p=0.0009) (**Fig 6J**). Thus, deprivation substantially decreased intrinsic excitability of L2/3 PV cells by increasing spike threshold, reducing spike probability, and delaying the time to first spike after current injection.

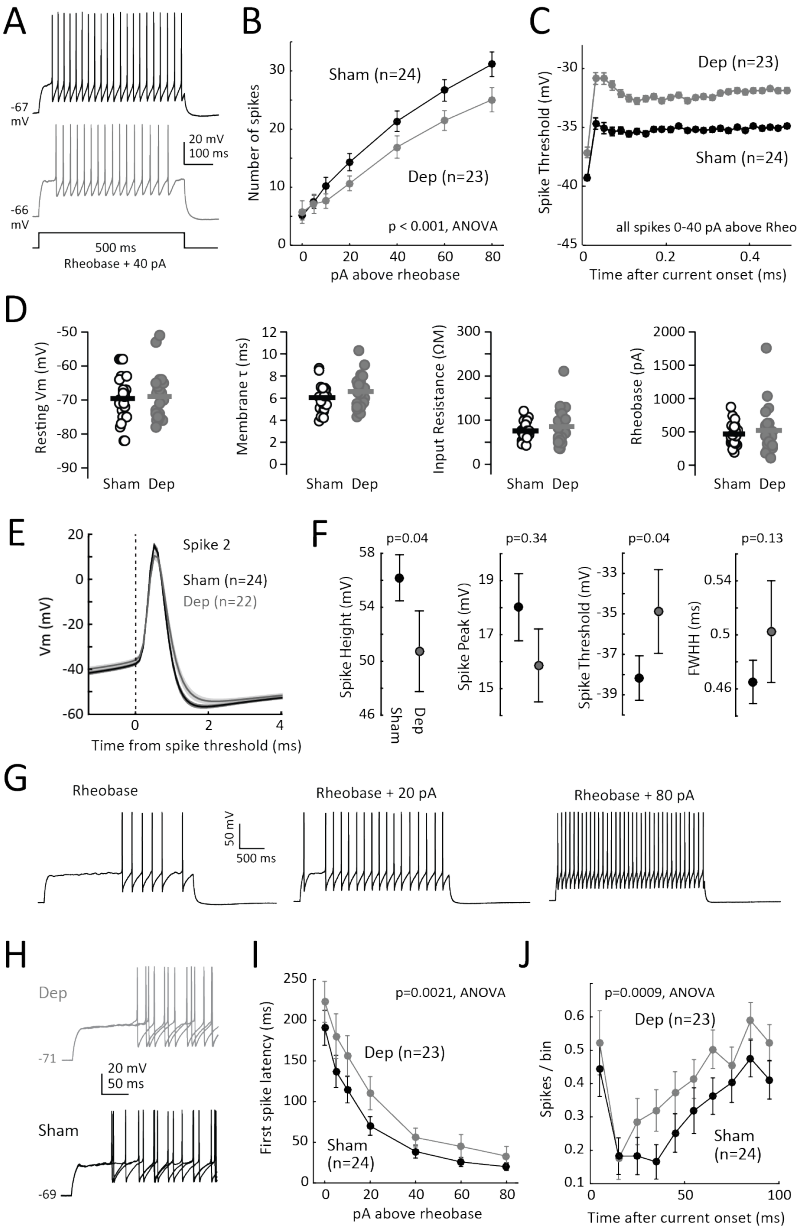

Figure 6. Deprivation causes a reduction in the intrinsic excitability of L2/3 PVs.
A, Spike trains for example sham (top) and deprived (bottom) L2/3 PV cells to current injection at 40 pA above rheobase. **B,** Mean F-I curve for spiking in sham and deprived PV cells. Symbols show mean +- SEM. **C,** Mean spike threshold, for all spikes recorded at 0-40 pA above rheobase, in 20 ms time bins. Many PV cells exhibit a rapid-onset first spike with systematically lower threshold (first point, see example in panel G). **D,** Resting properties and rheobase for each PV cell. Bars are means. **E,** Mean shape of 2nd spike at 80 pA above rheobase, across all cells. Shaded regions are +- sem. **F,** Quantification of spike shape for spikes at 80 pA above rheobase. p-values are from 2-tailed t-tests. **G,** Spike trains for an example PV cell showing delayed spike onset at rheobase. **H,** Spiking of an example sham (bottom) and deprived (top) PV cell at 5 pA above rheobase, showing longer spike latency in the deprived cell. **I,** Mean first spike latency in sham and deprived cells. **J,** Mean spike probability in 10-ms bins after current injection onset (20-80 pA above rheobase). p-values in I-J are for sham vs. deprived factor in 2-way ANOVA.

Deprivation up-regulates voltage-activated Kv currents in L2/3 PV cells

To investigate the mechanisms for reduced intrinsic excitability of L2/3 PV cells, we focused on two voltage-activated potassium currents that are known to regulate spike threshold in PV cells—the low-threshold, sustained delayed-rectifier potassium current (mediated by Kv1 channels) and the transient I_A current (mediated by Kv1.4 and Kv4 channels) (Gutman et al., 2005; Goldberg et al., 2008; Sun, 2009; Dehorter et al., 2015). Kv1 channels modulate spike threshold and first spike latency in PV cells (Goldberg et al., 2008; Dehorter et al., 2015), and their expression is bidirectionally regulated by large-scale manipulations of neural activity (Dehorter et al., 2015). I_A also regulates PV spike threshold, and may be altered by sustained whisker deprivation (Sun, 2009). Whether either is altered rapidly by brief sensory manipulations is unknown.

To measure delayed rectifier current, we used a whole-cell voltage clamp protocol that stepped Vhold from -70 mV to -10 mV in 10 mV steps (**Fig 7A-B**). The bath contained synaptic blockers (D-AP5, NBQX, saclofen, gabazine), the sodium channel blocker TTX (0.1 mM), the I_M blocker XE 991 (10 µM), the I_h blocker ZD2788 (0.1 mM), and low Ca^{2+} (0.5 mM) to reduce Ca-activated K currents. The K gluconate internal contained BAPTA to further reduce Ca-activated K currents. These conditions isolate delayed rectifier currents mediated by Kv1 and Kv2 families (which can be separated by activation threshold), and A-type currents that can be identified by their rapid inactivation. To further separate Kv1.1 from other currents, midway through each recording we washed in the blocker DTX-K at 0.1 mM, a Kv1.1-selective concentration (Robertson et al., 1996; Wang et al., 1999; Shen et al., 2004), and measured DTX-K-insensitive (non-Kv1.1) and DTX-K-sensitive currents. We obtained complete data from 13 Sham PV cells and 13 Deprived PV cells. Deprivation did not alter leak current (**Figure 7C**), but increased a steady-state K current that activated at -40 to -50 mV (**Figure 7D-E**, top row, $F(1,5)=5.16$, $p=0.025$, 2-factor ANOVA). This activation range is characteristic of Kv1-family channels (Coetzee et al., 1999). Steady-state currents in the presence of DTX-K were also significantly larger in deprived cells (**Figure 7D-E**, middle row, $F(1,5)=17.4$, $p=0.0001$), suggesting that non-Kv1.1 channel currents were up-regulated. DTX-K-sensitive currents, calculated by subtraction, were unchanged (**Figure 7D-E**, bottom row). These data indicate that a Kv1 channel, but not Kv1.1, is up-regulated by 1-day deprivation to reduce near-threshold excitability of L2/3 PV cells.

We examined I_A in separate experiments using a voltage protocol that isolates I_A based on its rapid inactivation at -40 mV (Guan et al., 2011) (**Figure 7F**). We stepped V_{hold} to 0 mV, which strongly activates I_A, either from a -70 mV prepulse, where I_A is not inactivated, or from a 200 ms -40 mV prepulse, which inactivates I_A. The bath contained synaptic blockers, TTX, 0.5 mM Ca^{2+} to reduced Ca-activated K currents, and 20 mM TEA to block most delayed rectifier K currents. Under these conditions, subtraction of -40 mV prepulse traces from -70 mV prepulse traces reveals I_A, which shows characteristic inactivation over ~30 ms (**Figure 7F**). Data were obtained from 16 Sham and 16 Deprived cells (6 mice each). I_A current magnitude was greater in Deprived PV cells than in Sham PV cells (sham: 10.5 ± 1.0 nA*ms, deprived: 14.2 ± 1.1 nA*ms, $t(30)=-2.4$, $p = 0.021$, t-test) (**Figure 7G-H**). Thus, both I_A and delayed rectifier currents were

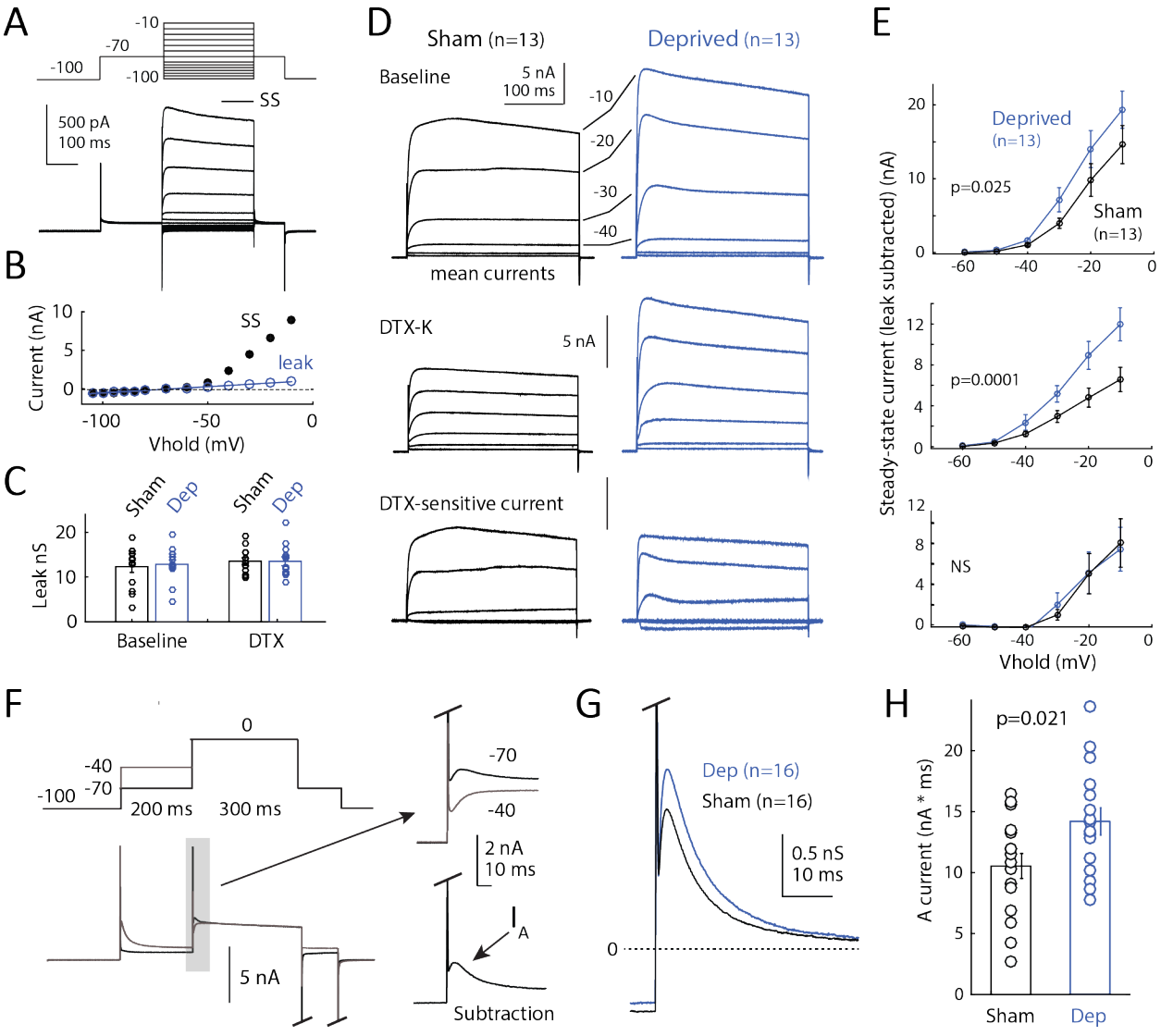

Figure 7. Deprivation up-regulates voltage-activated K currents in L2/3 PV cells. A, Voltage clamp protocol to measure delayed rectifier K currents, and example currents from one PV neuron in a Sham mouse. SS, steady-state current analysis window. **B,** I-V curve for steady-state (SS) and leak current for cell in (A). **C,** Leak conductance in Sham and Deprived cells, during baseline and DTX conditions. **D,** Mean current waveforms across Sham and Deprived PV cells at -60 to -10 mV Vhold, measured in baseline and DTX conditions (top and middle), and the calculated DTX-sensitive current (bottom). **E,** I-V plots for leak-subtracted steady-state current across cells, for each condition in (D). Pronounced currents activate at -40 to -50 mV. p-values are for Sham vs. Deprived factor in 2-way ANOVA. **F,** Voltage protocol for isolating I_A. I_A was measured at 0 mV by subtracting currents with a -40 mV 200-ms prestep (which inactivates I_A) from currents with a -70 mV preset (which does not). Traces show an example cell. **G,** Mean I_A waveform from Sham and Deprived cells. **F,** I_A magnitude (integrated over first 25 ms) for Sham and Deprived cells. Each circle is one cell. Bars show mean ± SEM.

increased by deprivation in L2/3 PV cells, which are expected to elevate spike threshold and reduce spike probability.

Functional effect of reduced inhibition on L2/3 PYR synaptic potentials

What is the functional effect of reduced PV-mediated inhibition on overall feedforward synaptic potentials (PSPs) in L2/3 PYR cells? This will depend on its coordination with the co-occurring reduction in feedforward excitation in these neurons. We first addressed this question using a standard parallel conductance model (Wehr and Zador, 2003; House et al., 2011) to predict the net PSP produced in each L2/3 PYR cell by the measured L4-evoked Gex and Gin waveforms at 1.4Eθ (data from **Figure 1**). The model calculates the PSP produced by Gex and Gin waveforms at a specific baseline Vm, given excitatory and inhibitory reversal potentials (0 and -68 mV). Input resistance and cell capacitance were set to the average values obtained from current clamp recordings (Sham: 95 MW, 240 pF, n=12 cells; Dep: 101 MW, 240 pF, n=13 cells). The model is passive and has no free parameters. We used a baseline Vm of -55 mV, to predict PSPs generated just below spike threshold, which may be most relevant to understand evoked spiking *in vivo*.

Figure 8A shows an example cell, with the predicted EPSP and IPSP generated by the measured Gex and Gin waveforms separately, and the total PSP predicted from Gex and Gin acting together. Deprived cells showed a significantly smaller predicted IPSP (from Gin alone) than sham cells (-5.4 ± 0.71 and -7.6 ± 0.95 mV, n=14 and 15, p=0.046, Wilcoxon rank-sum test), and a trend toward a smaller predicted EPSP (from Gex alone) (8.8 ± 1.6 and 13.2 ± 3.0 mV, p=0.16). This represents a similar average reduction in predicted IPSP and EPSP amplitude (29% and 33%, respectively) (**Figure 8B**). Predicted EPSP-IPSP ratio, quantified as E/(E+I) within each cell, was also unchanged (Sham: 0.60 ± 0.03, n=14; Dep: 0.61 ± 0.03, n=15, p=0.67). This contrasts with the preferential weakening of Gin over Gex at the conductance level (**Figure 1**). Modeling Gex and Gin together predicted a total PSP comprising a characteristic EPSP-IPSP sequence (Pouille and Scanziani, 2001; Gabernet et al., 2005; House et al., 2011). Strikingly, deprivation did not alter the predicted PSP peak, though the late hyperpolarization was reduced (**Figure 8C-D**). This indicates that deprivation-induced changes in Gin and Gex are quantitatively coordinated to maintain stability of peak feedforward PSPs in L2/3 PYR cells in the just-subthreshold regime.

To test the model predictions, we measured PSPs in L2/3 PYR cells in response to L4 stimulation at 1.4x Eθ, using K gluconate internal (n=12 Sham, n=13 Deprived). Current was injected somatically to achieve an estimated baseline synaptic Vm of -55 mV (see Methods). While PSP amplitude was heterogeneous across cells, the mean PSP consisted of an EPSP-IPSP sequence that was very similar to the modeled PSPs (**Figure 8E**). Confirming the model, deprivation did not alter PSP peak (p=0.68, Wilcoxon rank-sum test), but tended to reduce the late hyperpolarization phase of the PSP (non-significant trend, p=0.18) (**Figure 8F**). PSP duration was not significantly increased (width at half-height, Sham: 6.4 ± 2.4 ms, n=12; Dep: 9.6 ± 2.3 ms, n=13, p=0.19). Thus, deprivation-induced changes in Gin and Gex were functionally balanced for L2/3 PYR cells just below spike threshold, so that L4-evoked synaptic responses remained stable after deprivation, at least for low-frequency inputs.

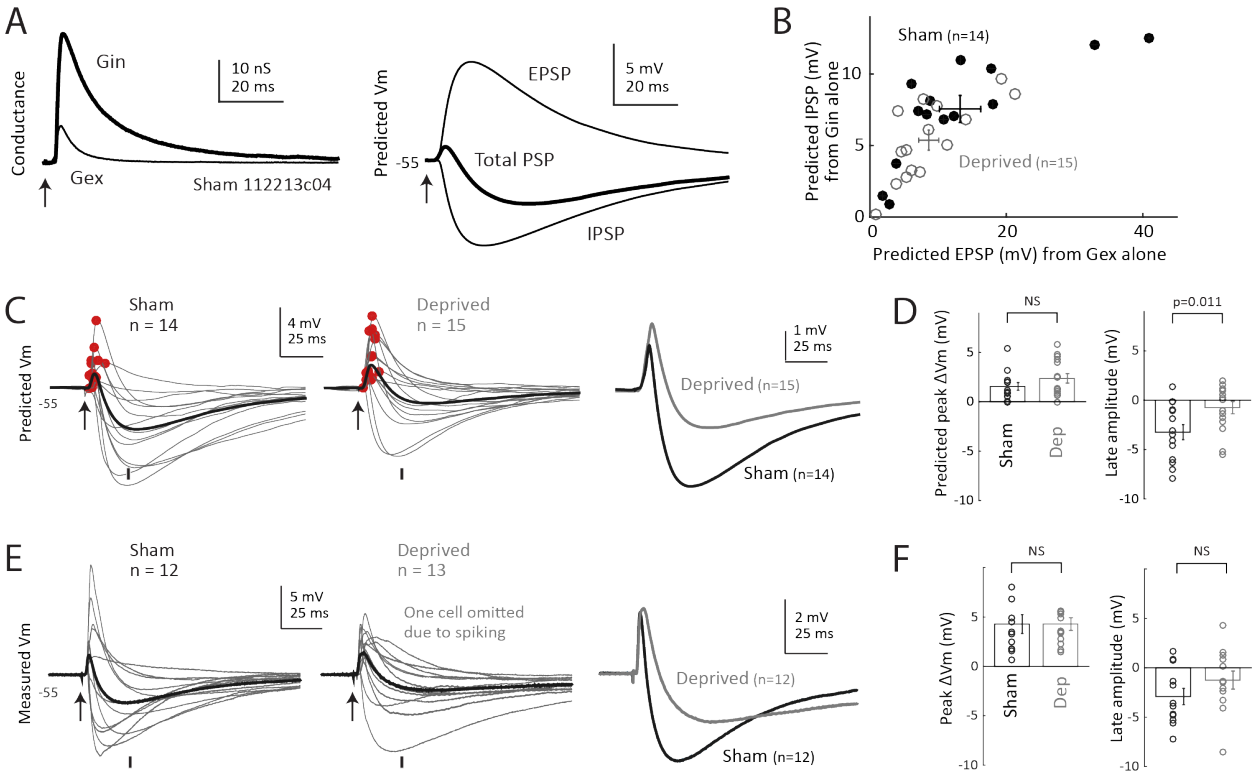

Figure 8. Changes in Gex and Gin are coordinated to maintain stable peak PSP amplitude in L2/3 PYR cells. A, Example neuron showing measured L4-evoked Gex and Gin conductance waveforms (left) and predicted PSPs from a baseline Vm of -55 mV (right). PSPs were predicted from Gex alone ("EPSP"), Gin alone ("IPSP"), or from both Gex and Gin together ("total PSP"). **B,** Peak predicted EPSP (from Gex alone) and IPSP (from Gin alone) at 1.4x Eθ in each Sham and Deprived cell from Figure 1. Error bars are mean ± SEM for Sham and Deprived populations. **C,** Predicted total PSP for each Sham and Deprived neuron, and population means (thick). Arrow, L4 stimulus. Dots, PSP peaks. Vertical tick, analysis time for late inhibition. Right, Population mean PSPs calculated from peak-aligned PSPs in individual cells. **D,** Quantification of changes in predicted peak PSP and late inhibition following deprivation. **E,** Real L4-evoked PSPs measured in sham and deprived L2/3 PYR neurons from estimated baseline synaptic Vm of -55 mV. Thick lines, population means. One deprived cell was omitted because it spiked. Right, Population mean PSPs calculated from peak-aligned PSPs in individual cells. **F,** Quantification of deprivation effects on peak PSP and late amplitude during the IPSP.

2.5 DISCUSSION

Whisker deprivation weakens PV-mediated feedforward inhibition in L2/3 of S1 in just 24 hrs, as rapidly as visual deprivation in V1 or hearing loss in A1 (Kuhlman et al., 2013; Sun et al., 2016; Resnik and Polley, 2017). Thus, rapid inhibitory circuit plasticity is common across sensory cortex. Optogenetic L4 stimulation showed that plasticity involves the L4-L2/3 feedforward microcircuit (**Figure 2**). However, because L2/3 PV neurons are shared between feedforward, recurrent and long-range projections, inhibition within all these circuits is likely to be reduced in L2/3 by whisker deprivation. Prior studies demonstrated plasticity on this 1-day time scale for inhibitory neuron axon/dendrite structure, inhibitory synapse number, and functional strength of PV input and output synapses (Knott et al., 2002; Maffei et al., 2006; 2010; Marik et al., 2010; Keck et al., 2011; Chen et al., 2012; van Versendaal et al., 2012; Chen and Nedivi, 2013; Kuhlman et al., 2013). Here we discovered equally rapid plasticity of PV intrinsic excitability. Thus, virtually every level of PV circuits exhibits rapid plasticity in response to sensory experience.

The cellular implementation of PV circuit plasticity appears to differ between cortical areas and with duration of deprivation. In rat S1, sustained (5+ day) whisker deprivation weakens L4-L2/3 feedforward inhibition by weakening L4 excitatory input to FS (presumed PV) neurons, with no change in FS intrinsic excitability (House et al., 2011). In mouse V1, 1-day monocular deprivation similarly weakens L4-evoked excitatory synaptic input to PV neurons (Kuhlman et al., 2013). However, 1-day whisker deprivation in mice changes neither net excitatory nor inhibitory synaptic input to PV neurons in S1, but instead reduces PV intrinsic excitability by increasing spike threshold (**Figures 4-6**). Thus, PV circuits appear to utilize different plasticity mechanisms to achieve a similar overall reduction in circuit output. Our findings suggest that within S1, the most rapid mechanism for disinhibition in L2/3 is reduction in PV intrinsic excitability, followed more slowly by weakening of L4 excitatory synapses onto PV neurons.

PV intrinsic excitability is plastic in response to strong or prolonged genetic or pharmacological suppression or enhancement of cortical activity (Miller et al., 2011; Dehorter et al., 2015) and epilepsy (Li et al., 2011). Our results show that this plasticity also occurs to natural variations in sensory use, and thus is a normally occurring, rapid plasticity mechanism in cortex.

Mechanism for altered PV intrinsic excitability

Deprivation altered intrinsic excitability of PV cells near spike threshold, but not at rest. Near-threshold excitability is strongly regulated in L2/3 PV neurons by low-threshold Kv1 delayed rectifier channels, which help set spike threshold and spike latency (Goldberg et al., 2008). Recent studies identified molecular pathways for slower activity-dependent regulation of Kv1 currents, via the transcription factor Er81 (Dehorter et al., 2015), or by neuregulin (NRG1) signaling through its receptor ErbB4 (Li et al., 2011). Modulation of PV cell activity by direct genetic or pharmacological interventions (Dehorter et al., 2015), epilepsy (Li et al., 2011) or synaptic stimulation (Campanac et al., 2013) regulates Kv1 channels to alter near-threshold PV

intrinsic excitability. Our results are consistent with this same mechanism occurring rapidly during sensory deprivation, because deprivation increased a voltage activated sustained current that activated near spike threshold (-40 mV), characteristic of Kv1 family channels (**Figure 7**). The molecular identity of the channels that mediate this current remains unknown, but it likely involves a Kv1 family member that is not Kv1.1. Thus, we propose that activity-dependent modulation of Kv1 function, previously observed during artificial activity manipulation or epilepsy, is recruited with brief alterations of sensory experience to regulate PV circuit function.

Deprivation also increased A-type potassium currents (I_A). Upregulation of I_A was suggested previously to occur in L4 fast-spiking neurons after prolonged (30 day) whisker deprivation, and to cause elevated spike threshold and spike latency (Sun, 2009). We find this occurs within 1 day of deprivation. Thus, multiple Kv channels are rapidly regulated in PV cells by whisker experience to change near-threshold but not resting excitability.

What signaling pathways mediate experience-dependent regulation of potassium channel function in PV neurons? This is unknown, but one candidate is NRG1/ErbB4 signaling, which controls many aspects of PV circuit development and plasticity (Mei and Nave, 2014). NRG1/ErbB4 is required for visual deprivation-induced weakening of PV circuits (Sun et al., 2016) and for epilepsy-dependent regulation of PV intrinsic excitability (Li et al., 2011).

PV circuit weakening and sensory response homeostasis in L2/3 of S1

Rapid weakening of PV circuits contributes to homeostatic stabilization of sensory-evoked spiking in L2/3 PYR cells, observed following brief reductions in whisker input. In classical whisker map plasticity, ≥5 days of D-row whisker deprivation weakens spiking to deprived whiskers in L2/3 PYR cells, mediated in part by long-term depression (LTD) at excitatory L4-L2/3 PYR synapses (Fox, 2002; Feldman, 2009). With briefer 1-3 d whisker deprivation, whisker-evoked spiking remains normal or is slightly increased, even though whisker-evoked synaptic excitation is already weakened in L2/3 PYR cells. This is due to a substantial drop in whisker-evoked inhibition in L2/3 PYR cells, measured with whole-cell recording *in vivo* (Li et al., 2014). Our results identify the circuit loci for this plasticity within L4-L2/3 feedforward excitatory and inhibitory circuits. Deprivation weakens L4-L2/3 feedforward excitation onto PYR cells in < 1 day (**Figures 1-2**), as expected for a rapid LTD process, and similar to visual deprivation-induced LTD in L2/3 of V1 (Heynen et al., 2003). At the same time, L4-L2/3 feedforward inhibition is weakened more strongly, by rapid reduction in PV intrinsic excitability, and this precisely counteracts the loss of feedforward excitation onto L2/3 PYR cells, thus preserving L4-evoked PSPs (**Figure 8**). The LTD and PV intrinsic excitability mechanisms operate within different neurons, and therefore must be coordinated to accurately stabilize L2/3 PYR synaptic and spiking responses, but how this is achieved is unknown.

We found that 1 day deprivation reduces feedforward Gin preferentially over Gex in L2/3 PYR cells, elevating E-I conductance ratio. Remarkably, this change in E-I conductance ratio is

appropriate to maintain stable feedforward PSP magnitude, for cells just below spike threshold (**Figure 8**). This is because in this Vm regime, driving force on inhibition is lower than excitation, so a larger change is required in Gin than Gex to produce an equivalent change (DVm) in IPSP vs. EPSP amplitude, which approximately sum to yield a stable PSP peak. Thus, rapid plasticity of L2/3 PV intrinsic excitability appears calibrated to homeostatically maintain stable feedforward synaptic responses in the L2/3 PYR network. This explains why whisker-evoked spiking responses in L2/3 remain largely stable following brief whisker deprivation *in vivo* (Li et al., 2014). Interestingly, while brief deprivation preserves short-latency whisker-evoked spiking in L2/3 *in vivo*, it modestly increases long-latency spikes and spike jitter (Li et al., 2014), which may reflect the modest broadening of the PSP peak or loss of the late IPSP (**Figure 8**). With longer (≥5 days) deprivation, feedforward Gex and Gin are reduced equally in L2/3 PYR cells, which predicts a smaller feedforward net PSP (House et al., 2011). This may explain the loss of whisker-evoked spikes in L2/3 during classical map plasticity (Li et al., 2014).

Longer deprivation drives other mechanisms for activity-dependent weakening of PV circuits, including weakening of excitatory synaptic input to PV cells (House et al., 2011; Kuhlman et al., 2013; Sun et al., 2016) and weakening of unitary PV→PYR output synapses (Xue et al., 2014). How different plasticity mechanisms are coordinated within PV circuits remains unclear.

Rapid disinhibition has several advantages as a mechanism for network homeostasis. It is faster than classical homeostatic synaptic scaling or homeostatic plasticity of PYR intrinsic excitability, which take 2-3 days to occur *in vivo* (Breton and Stuart, 2009; Lambo and Turrigiano, 2013; Gainey and Feldman, 2017). It is highly efficient, because plasticity in a single PV cell will regulate firing rate in hundreds of local PYR cells (Packer and Yuste, 2011). It also doesn't require broad adjustment of synaptic strength at hundreds or thousands of excitatory input synapses onto PV cells (Sun et al., 2016). We speculate that global adjustment of PV circuit gain by regulation of PV intrinsic excitability may provide coarse regulation of excitation-inhibition balance, which is followed by slower, more precise adjustment of unitary PV→PYR synapses for target-cell specific regulation (Xue et al., 2014). Vasoactive intestinal peptide (VIP) interneuron circuits provide even faster, dynamic disinhibition (time scale of seconds), but whether these circuits are plastic in response to experience is unknown (Fu et al., 2015).

While reduced PV intrinsic excitability preserves the net feedforward PSP peak, the late IPSP component shows a strong tendency to be reduced (**Figure 8**). This suggests that while PV circuit plasticity promotes stable synaptic responses to sparse, low-frequency input (which is the dominant activity regime in L2/3 of S1 (Barth and Poulet, 2012)), it may also result in increased depolarization in L2/3 PYR cells during high-frequency input trains, due to enhanced temporal summation. This may facilitate long-term potentiation and Hebbian map reorganization (Kuhlman et al., 2013; Gambino et al., 2014), similar to VIP-mediated disinhibition on short time scales (Williams and Holtmaat, 2018).

2.6 ACKNOWLEDGEMENTS

This chapter, in full, is a republication of the material as it appears in Gainey, M. A., Aman, J. W., & Feldman, D. E. (2018). Rapid Disinhibition by Adjustment of PV Intrinsic Excitability during Whisker Map Plasticity in Mouse S1. The Journal of Neuroscience, 38(20), 4749–4761. The dissertation author was the second author of this paper. M.A.G. designed research, performed experiments, analyzed and interpreted data, and contributed to writing the paper. J.W.A. was solely responsible for the series of experiments presented in Figure 2, including experiment design, data collection, data analysis, interpretation, and writing. D.E.F. designed research, analyzed data, and contributed to writing the paper.

This work was supported by NIH 1R01NS073912, F32 NS087893 (to MAG), and a NSF Graduate Research Fellowship (to JWA). We thank Brooke Angel and Dhruv Malik for histology and solution making.

2.7 REFERENCES

Adesnik H, Scanziani M (2010) Lateral competition for cortical space by layer-specific horizontal circuits. Nature 464:1155–1160.

Allen CB, Celikel T, Feldman DE (2003) Long-term depression induced by sensory deprivation during cortical map plasticity in vivo. Nature Neuroscience 6:291–299.

Barnes SJ, Sammons RP, Jacobsen RI, Mackie J, Keller GB, Keck T (2015) Subnetwork-Specific Homeostatic Plasticity in Mouse Visual Cortex In Vivo. Neuron 86:1290–1303.

Barth AL, Poulet JFA (2012) Experimental evidence for sparse firing in the neocortex. Trends Neurosci 35:345–355.

Breton J-D, Stuart GJ (2009) Loss of sensory input increases the intrinsic excitability of layer 5 pyramidal neurons in rat barrel cortex. J Physiol (Lond) 587:5107–5119.

Campanac E, Gasselin C, Baude A, Rama S, Ankri N, Debanne D (2013) Enhanced intrinsic excitability in basket cells maintains excitatory-inhibitory balance in hippocampal circuits. Neuron 77:712–722.

Chen JL, Nedivi E (2013) Highly specific structural plasticity of inhibitory circuits in the adult neocortex. Neuroscientist 19:384–393.

Chen JL, Villa KL, Cha JW, So PTC, Kubota Y, Nedivi E (2012) Clustered dynamics of inhibitory synapses and dendritic spines in the adult neocortex. Neuron 74:361–373.

Coetzee WA, Amarillo Y, Chiu J, Chow A, Lau D, McCormack T, Moreno H, Nadal MS, Ozaita A, Pountney D, Saganich M, Vega-Saenz de Miera E, Rudy B (1999) Molecular diversity of K+ channels. Ann N Y Acad Sci 868:233–285.

Dehorter N, Ciceri G, Bartolini G, Lim L, del Pino I, Marín O (2015) Tuning of fast-spiking interneuron properties by an activity-dependent transcriptional switch. Science 349:1216–1220.

Donato F, Rompani SB, Caroni P (2013) Parvalbumin-expressing basket-cell network plasticity induced by experience regulates adult learning. Nature 504:272–276.

Feldman DE (2009) Synaptic mechanisms for plasticity in neocortex. Annu Rev Neurosci 32:33–55.

Finnerty GT, Roberts LS, Connors BW (1999) Sensory experience modifies the short-term dynamics of neocortical synapses. Nature 400:367–371.

Fox K (2002) Anatomical pathways and molecular mechanisms for plasticity in the barrel cortex. Neuroscience 111:799–814.

Fritschy J-M, Panzanelli P (2014) GABAA receptors and plasticity of inhibitory neurotransmission in the central nervous system. Eur J Neurosci 39:1845–1865.

Froemke RC (2015) Plasticity of cortical excitatory-inhibitory balance. Annu Rev Neurosci 38:195–219.

Fu Y, Kaneko M, Tang Y, Alvarez-Buylla A, Stryker MP (2015) A cortical disinhibitory circuit for enhancing adult plasticity. Elife 4:e05558.

Gabernet L, Jadhav SP, Feldman DE, Carandini M, Scanziani M (2005) Somatosensory integration controlled by dynamic thalamocortical feed-forward inhibition. Neuron 48:315–327.

Gainey MA, Feldman DE (2017) Multiple shared mechanisms for homeostatic plasticity in rodent somatosensory and visual cortex. Philos Trans R Soc Lond, B, Biol Sci 372.

Gambino F, Holtmaat A (2012) Spike-timing-dependent potentiation of sensory surround in the somatosensory cortex is facilitated by deprivation-mediated disinhibition. Neuron 75:490–502.

Gambino F, Pages S, Kehayas V, Baptista D, Tatti R, Carleton A, Holtmaat A (2014) Sensory-evoked LTP driven by dendritic plateau potentials in vivo. Nature 515:116–119.

Gibson JR, Beierlein M, Connors BW (1999) Two networks of electrically coupled inhibitory neurons in neocortex. Nature 402:75–79.

Goldberg EM, Clark BD, Zagha E, Nahmani M, Erisir A, Rudy B (2008) K+ channels at the axon initial segment dampen near-threshold excitability of neocortical fast-spiking GABAergic interneurons. Neuron 58:387–400.

Guan D, Horton LR, Armstrong WE, Foehring RC (2011) Postnatal development of A-type and Kv1- and Kv2-mediated potassium channel currents in neocortical pyramidal neurons. J Neurophysiol 105:2976–2988.

Gutman GA, Chandy KG, Grissmer S, Lazdunski M, McKinnon D, Pardo LA, Robertson GA, Rudy B, Sanguinetti MC, Stuhmer W, Wang X (2005) International Union of Pharmacology. LIII. Nomenclature and molecular relationships of voltage-gated potassium channels. Pharmacol Rev 57:473–508.

Helmstaedter M, Staiger JF, Sakmann B, Feldmeyer D (2008) Efficient recruitment of layer 2/3 interneurons by layer 4 input in single columns of rat somatosensory cortex. Journal of Neuroscience 28:8273–8284.

Hengen KB, Lambo ME, Van Hooser SD, Katz DB, Turrigiano GG (2013) Firing rate homeostasis in visual cortex of freely behaving rodents. Neuron 80:335–342.

Heynen AJ, Yoon B-J, Liu C-H, Chung HJ, Huganir RL, Bear MF (2003) Molecular mechanism for loss of visual cortical responsiveness following brief monocular deprivation. Nature Neuroscience 6:854–862.

Hippenmeyer S, Vrieseling E, Sigrist M, Portmann T, Laengle C, Ladle DR, Arber S (2005) A developmental switch in the response of DRG neurons to ETS transcription factor signaling. PLoS Biol 3:e159.

House DRC, Elstrott J, Koh E, Chung J, Feldman DE (2011) Parallel regulation of feedforward inhibition and excitation during whisker map plasticity. Neuron 72:819–831.

Jiao Y, Zhang C, Yanagawa Y, Sun Q-Q (2006) Major effects of sensory experiences on the neocortical inhibitory circuits. Journal of Neuroscience 26:8691–8701.

Kätzel D, Zemelman BV, Buetfering C, Wölfel M, Miesenböck G (2011) The columnar and laminar organization of inhibitory connections to neocortical excitatory cells. Nature Neuroscience 14:100–107.

Keck T, Scheuss V, Jacobsen RI, Wierenga CJ, Eysel UT, Bonhoeffer T, Hübener M (2011) Loss of sensory input causes rapid structural changes of inhibitory neurons in adult mouse visual cortex. Neuron 71:869–882.

Knott GW, Quairiaux C, Genoud C, Welker E (2002) Formation of dendritic spines with GABAergic synapses induced by whisker stimulation in adult mice. Neuron 34:265–273.

Kuhlman SJ, Olivas ND, Tring E, Ikrar T, Xu X, Trachtenberg JT (2013) A disinhibitory microcircuit initiates critical-period plasticity in the visual cortex. Nature 501:543–546.

Lambo ME, Turrigiano GG (2013) Synaptic and Intrinsic Homeostatic Mechanisms Cooperate to Increase L2/3 Pyramidal Neuron Excitability during a Late Phase of Critical Period Plasticity. Journal of Neuroscience 33:8810–8819.

Li K-X, Lu Y-M, Xu Z-H, Zhang J, Zhu J-M, Zhang J-M, Cao S-X, Chen X-J, Chen Z, Luo J-H, Duan S, Li X-M (2011) Neuregulin 1 regulates excitability of fast-spiking neurons through Kv1.1 and acts in epilepsy. Nature Neuroscience 15:267–273.

Li L, Gainey MA, Goldbeck JE, Feldman DE (2014) Rapid homeostasis by disinhibition during whisker map plasticity. Proc Natl Acad Sci USA 111:1616–1621.

Madisen L, Zwingman TA, Sunkin SM, Oh SW, Zariwala HA, Gu H, Ng LL, Palmiter RD, Hawrylycz MJ, Jones AR, Lein ES, Zeng H (2010) A robust and high-throughput Cre reporting and characterization system for the whole mouse brain. Nature Neuroscience 13:133–140.

Maffei A, Lambo ME, Turrigiano GG (2010) Critical period for inhibitory plasticity in rodent binocular V1. Journal of Neuroscience 30:3304–3309.

Maffei A, Nataraj K, Nelson SB, Turrigiano GG (2006) Potentiation of cortical inhibition by visual deprivation. Nature 443:81–84.

Maffei A, Nelson SB, Turrigiano GG (2004) Selective reconfiguration of layer 4 visual cortical circuitry by visual deprivation. Nature Neuroscience 7:1353–1359.

Marik SA, Yamahachi H, McManus JNJ, Szabo G, Gilbert CD (2010) Axonal dynamics of excitatory and inhibitory neurons in somatosensory cortex. PLoS Biol 8:e1000395.

Mateo C, Avermann M, Gentet LJ, Zhang F, Deisseroth K, Petersen CCH (2011) In vivo optogenetic stimulation of neocortical excitatory neurons drives brain-state-dependent inhibition. Curr Biol 21:1593–1602.

Mei L, Nave K-A (2014) Neuregulin-ERBB signaling in the nervous system and neuropsychiatric diseases. Neuron 83:27–49.

Miller MN, Okaty BW, Kato S, Nelson SB (2011) Activity-dependent changes in the firing properties of neocortical fast-spiking interneurons in the absence of large changes in gene expression. Dev Neurobiol 71:62–70.

Packer AM, Yuste R (2011) Dense, unspecific connectivity of neocortical parvalbumin-positive interneurons: a canonical microcircuit for inhibition? Journal of Neuroscience 31:13260–13271.

Pouille F, Scanziani M (2001) Enforcement of temporal fidelity in pyramidal cells by somatic feed-forward inhibition. Science 293:1159–1163.

Resnik J, Polley DB (2017) Fast-spiking GABA circuit dynamics in the auditory cortex predict recovery of sensory processing following peripheral nerve damage. Elife 6.

Robertson B, Owen D, Stow J, Butler C, Newland C (1996) Novel effects of dendrotoxin homologues on subtypes of mammalian Kv1 potassium channels expressed in Xenopus oocytes. FEBS Lett 383:26–30.

Shao YR, Isett BR, Miyashita T, Chung J, Pourzia O, Gasperini RJ, Feldman DE (2013) Plasticity of recurrent l2/3 inhibition and gamma oscillations by whisker experience. Neuron 80:210–222.

Shen W, Hernandez-Lopez S, Tkatch T, Held JE, Surmeier DJ (2004) Kv1.2-containing K+ channels regulate subthreshold excitability of striatal medium spiny neurons. J Neurophysiol 91:1337–1349.

Shepherd GMG, Pologruto TA, Svoboda K (2003) Circuit analysis of experience-dependent plasticity in the developing rat barrel cortex. Neuron 38:277–289.

Sun Q-Q (2009) Experience-dependent intrinsic plasticity in interneurons of barrel cortex layer IV. J Neurophysiol 102:2955–2973.

Sun Y, Ikrar T, Davis MF, Gong N, Zheng X, Luo ZD, Lai C, Mei L, Holmes TC, Gandhi SP, Xu X (2016) Neuregulin-1/ErbB4 Signaling Regulates Visual Cortical Plasticity. Neuron 92:160–173.

Turrigiano GG (2017) The dialectic of Hebb and homeostasis. Philos Trans R Soc Lond, B, Biol Sci 372.

van Versendaal D, Rajendran R, Saiepour MH, Klooster J, Smit-Rigter L, Sommeijer J-P, De Zeeuw CI, Hofer SB, Heimel JA, Levelt CN (2012) Elimination of inhibitory synapses is a major component of adult ocular dominance plasticity. Neuron 74:374–383.

Wang FC, Bell N, Reid P, Smith LA, McIntosh P, Robertson B, Dolly JO (1999) Identification of residues in dendrotoxin K responsible for its discrimination between neuronal K+ channels containing Kv1.1 and 1.2 alpha subunits. Eur J Biochem 263:222–229.

Wehr M, Zador AM (2003) Balanced inhibition underlies tuning and sharpens spike timing in auditory cortex. Nature 426:442–446.

Williams LE, Holtmaat A (2018) Higher-order thalamocortical inputs gate synaptic long-term potentiation via disinhibiton. bioRxiv 281477; doi: https://doi.org/10.1101/281477.

Xue M, Atallah BV, Scanziani M (2014) Equalizing excitation-inhibition ratios across visual cortical neurons. Nature 511:596–600.

Chapter 3

Whisker deprivation drives multiple timescales of PV interneuron plasticity in mouse S1

Joseph W. Aman & Daniel E. Feldman

3.1 SUMMARY

Sensory deprivation drives Hebbian and homeostatic plasticity in sensory cortex that can have distinct temporal components, but the time course of plasticity within inhibitory circuits is poorly understood. In rodent somatosensory cortex (S1), whisker deprivation drives homeostatic plasticity within parvalbumin (PV) interneuron circuits that rapidly decreases feedforward PV-mediated inhibition, thus stabilizing whisker-evoked firing of L2/3 pyramidal neurons (Li et al., 2014). A major component of this PV circuit homeostasis is a decrease in the intrinsic excitability of L2/3 PV interneurons, which occurs with 1 day of deprivation. Prior work showed that this is mediated by an increase in PV spike threshold due to enhanced Kv1 potassium currents, with no change in excitability near Vrest (Gainey, Aman, & Feldman, 2018). Here, we asked whether longer, 3-day deprivation recruited different or additional mechanisms to modulate PV intrinsic excitability. We plucked the D row of whiskers for 1 or 3 days, starting at P15-20, in PV-Cre/tdTomato mice, and prepared ex vivo S1 slices at P18-P23. Whole-cell recordings from L2/3 PV neurons in D columns showed that similar to prior findings with 1-day deprivation, 3-day deprivation reduced spiking in F-I curves relative to age-matched sham-deprived littermates. In contrast to prior findings with 1-day deprivation, 3-day deprivation had no effect on spike threshold, but did cause an increase in input resistance at Vrest. Furthermore, 3-day deprivation enhanced the medium afterhyperpolarization (mAHP), which explained the decreased spike rate in F-I curves. This increase in mAHP was not observed with 1-day deprivation. Thus, different cell physiological changes underlie decreased PV cell excitability after 1-day and 3-day whisker deprivation. This suggests that experience-dependent plasticity of cortical inhibitory circuits involves a cascade of temporally distinct components.

3.2 INTRODUCTION

Changes in sensory experience induce a diversity of plasticity mechanisms in neural circuits. Often, a single sensory manipulation drives a succession of multiple distinct processes. In one classical example, monocular deprivation drives ocular dominance plasticity in V1 that involves a cascade of different synaptic and cellular plasticity mechanisms, beginning with rapid long-term depression (LTD) of excitatory synapses conveying closed-eye input, followed by homeostatic synaptic scaling that increases the strength of all synapses and is responsible for the increase in open-eye responses in V1 (Espinosa & Stryker, 2012). Similarly in S1, whisker deprivation causes adaptive shifts in whisker receptive fields that are caused by a rapid depression of responses to deprived whiskers (which involves LTD), followed several days later by an enhancement of responses to spared whiskers (which involves LTP) (Fox, 2002; Feldman, 2009). In other cases, multiple cellular mechanisms can be induced simultaneously by a single sensory or activity manipulation (e.g., suppressing activity in cortical pyramidal cells drives both scaling-up of excitatory synapses and increased intrinsic excitability in pyramidal cells, as compensatory mechanisms (Wen & Turrigiano, 2021). Thus, cortical circuits, and even single neurons, possess multiple plasticity mechanisms, several of which can be recruited at once, or in sequence, during sensory-dependent plasticity or homeostasis.

In contrast to excitatory circuits, much less is known about experience-dependent plasticity in cortical inhibitory circuits. An important inhibitory cell type is the parvalbumin-positive (PV) interneuron, which provides fast, highly sensitive inhibition in feedforward and feedback circuits (Isaacson & Scanziani, 2011). PV circuits in L2/3 of sensory cortex show rapid plasticity in response to changes in sensory input. Brief (1–3 day) sensory deprivation rapidly decreases PV circuit function, as assessed by a reduction in sensory-evoked PV spiking and reduced sensory-evoked inhibition in pyramidal (PYR) cells (Kuhlman et al., 2013; L. Li, Gainey, Goldbeck, & Feldman, 2014; Resnik & Polley, 2017). This occurs after visual deprivation in V1 (Hengen, Lambo, Van Hooser, Katz, & Turrigiano, 2013; Kuhlman et al., 2013), after whisker deprivation in S1 (L. Li et al., 2014), and after hearing loss in auditory cortex (Resnik & Polley, 2017). The function of this rapid reduction in PV circuit function is debated. Reduced PV inhibition can act to facilitate Hebbian plasticity, and thus may be a gate to allow subsequent reorganization of excitatory circuits (Harauzov et al., 2010; Gambino & Holtmaat, 2012; Barnes et al., 2015). But in addition, the weakening of PV inhibition after deprivation could have a homeostatic function, to disinhibit PYR cells and thereby maintain average PYR cell firing rates despite the loss of excitatory sensory drive (Hengen et al., 2013; L. Li et al., 2014; Barnes et al., 2015; Gainey & Feldman, 2017). This active maintenance of PYR firing rate, termed firing rate homeostasis, is a robust response to changing sensory use and involves homeostatic changes in both inhibitory and excitatory circuits (Gainey & Feldman, 2017; Turrigiano, 2017).

The current study focuses on cellular mechanisms for rapid PV circuit homeostasis in sensory cortex. The mechanisms that underlie rapid deprivation-induced changes in PV circuit function are incompletely understood, in part because many previous studies have focused on long-term sensory deprivation (Yazaki-Sugiyama, Kang, Câteau, Fukai, & Hensch, 2009; Kameyama et al.,

2010; House, Elstrott, Koh, Chung, & Feldman, 2011). In principle, reduced PV circuit function following sensory deprivation could involve reduced excitatory synaptic input to PV cells, decreased PV intrinsic excitability, decreased inhibitory synaptic output, or increased inhibition of PV cells. In primary visual (V1) cortex, 1–2 days of deprivation drives a loss of inhibitory cell spines and a decrease in inhibitory synapse number (Keck et al., 2011; Chen et al., 2012; van Versendaal et al., 2012; Villa et al., 2016). Rapid PV disinhibition in V1 is also associated with a decrease in excitatory synaptic strength onto L2/3 PV neurons (Kuhlman et al., 2013; Y. Sun et al., 2016). In primary somatosensory (S1) cortex, whisker deprivation reduces inhibitory bouton density in deprived whisker columns within hours, suggesting a loss of functional inhibitory synapses (Marik, Yamahachi, McManus, Szabo, & Gilbert, 2010). In contrast with V1, recent work in S1 found that 1 day of D-row whisker deprivation did not affect excitatory drive to L2/3 PV cells (Gainey et al., 2018). Instead, deprivation decreased the intrinsic excitability of L2/3 PV cells, leading to decreased PV spiking and a decrease in inhibition in L2/3 PYR cells.

The diversity of neuronal ion channels, and particularly K channels, with different voltage-dependent properties provides a wide variety of ways that intrinsic excitability can be regulated—e.g., by regulating resting potential or input resistance, or by regulating spike threshold, or by regulating AHPs that govern inter-spike interval. 1-day deprivation in S1 was shown to reduce PV intrinsic excitability specifically by altering spike threshold without changing resting properties. This occurred because 1 day of deprivation increased Kv1 currents and A-type K currents, both of which are activated near threshold and control spike threshold (Gainey et al., 2018; Gutman et al., 2005). In pyramidal cells, experience and circuit activity can regulate a wide variety of intrinsic conductances, suggesting that many different solutions to changing intrinsic excitability are available to neurons. What other mechanisms exist for plasticity of intrinsic excitability in PV neurons is not well understood.

We hypothesized that additional plasticity mechanisms may be recruited in L2/3 PV neurons in response to different time scales of whisker deprivation. To test this, we extended the duration of whisker deprivation to 3 days and asked whether changes in L2/3 PV circuits were consistent with those observed after 1 day of deprivation. While the effects of 3 day deprivation have not been studied in mice, work in rats shows that whisker-evoked inhibition is reduced by 3-day deprivation even more than by 1-day deprivation (L. Li et al., 2014). But how PV circuits are specifically affected by 3-day deprivation is unknown. We hypothesize that 1 day and 3 day deprivation drive distinct physiological changes in L2/3 PV neurons.

3.3 MATERIALS & METHODS

Procedures were approved by the University of California, Berkeley Animal Care and Use Committee and followed National Institutes of Health guidelines. Homozygous Pvalb-IRES-Cre mice (Hippenmeyer et al., 2005) were crossed with homozygous Ai14 tdTomato Cre reporter mice (Madisen et al., 2010) to generate PV-Cre;tdTomato offspring. Mice were housed as litters in standard cages on a 12:12-hr light-dark cycle. For whisker deprivation, the right D-row

whiskers (D1–D6 and gamma) were plucked under transient isoflurane anesthesia. Sham littermates underwent anesthesia but not plucking. Slice physiology experiments used mice of either sex aged P18–P23. Recordings were performed during the dark phase of the light cycle.

Slice preparation

Mice were anesthetized with isoflurane and decapitated. The brain was sliced using a Leica VT1200S vibratome in chilled, oxygenated, low-sodium, low-calcium Ringer's solution (in mm: 85 NaCl, 75 sucrose, 25 D-(+)-glucose, 4 $MgSO_4$, 2.5 KCl, 1.25 Na_2HPO_4, 0.5 ascorbic acid, 25 $NaHCO_3$, and 0.5 $CaCl_2$, 320 mOsm). Cortical slices 350 µm thick were cut from the left hemisphere in the "across-row" plane, oriented 50° from the midsagittal plane and 35° from the vertical plane. Using this slicing method, each slice contains one barrel column from each whisker row (A–E) (Finnerty, Roberts, & Connors, 1999; Allen, Celikel, & Feldman, 2003; Gainey et al., 2018). Slices were then incubated at 32°C for 30 min in standard Ringer's solution (in mM: 119 NaCl, 2.5 KCl, 1.3 $MgSO_4$, 1 NaH_2PO_4, 26.2 $NaHCO_3$, 11 D-(+)-glucose and 2.5 $CaCl_2$; pH 7.3, 300 mOsm, and bubbled with 95% O_2 and 5% CO_2). Slices were maintained at room temperature > 30 min before recording.

Electrophysiology

Recordings were made at 30–31°C in standard Ringer's solution, perfused at 2.5-3.0 mL/min. All recordings were made in L2/3 of D-row barrel columns. Barrels were visualized by transillumination at 4x and whole-cell recordings were targeted using infrared differential interference contrast (DIC) optics at 40x. L2/3 PYR cells were identified visually using soma shape, and L2/3 PV cells were identified by tdTomato fluorescence (Olympus U-MNG2 filter cube: 530–550 nm bandpass excitation, 590 nM emission; Rolera-XR camera; visualized by MicroManager imaging software).

Current clamp recordings used potassium gluconate internal solution (in mM: 116 K gluconate, 20 HEPES, 6 KCl, 2 NaCl, 0.5 EGTA, 4 MgATP, 0.3 NaGTP, 105 Na phosphocreatine, pH 7.20, 290 mOsm). For voltage clamp recordings of synaptic currents, we used cesium gluconate internal solution (in mM: 108 D-gluconic acid, 108 CsOH, 20 HEPES, 5 tetraethylammonium-Cl, 2.8 NaCl, 0.4 EGTA, 4 MgATP, 0.3 NaGTP, 5 BAPTA, 5 QX314 bromide (adjusted to pH 7.2 with CsOH, 290 mOsm). Whole-cell recordings were made using 3–5 MΩ pipettes. Cells were discarded if uncompensated series resistance (Rseries) was > 15 MΩ or if resting membrane potential (Vrest) at break-in was > -60 mV. Recordings were made using a Multiclamp 700B amplifier (Molecular Devices). Signals were low-pass filtered (2–4 kHz) and digitized (10-20 kHz). Data acquisition used custom software in IGOR Pro (Wavemetrics).

PV intrinsic excitability

PV cells were recorded in whole-cell current-clamp mode. Glutamate and GABA-A receptors were blocked with the addition of 50 µM D-AP5 (Cayman Chemical #14539), 10 µM NBQX

disodium salt (Abcam #ab120045), and 3 µM Gabazine (Tocris Bioscience #1262) to the extracellular solution. Vrest was measured immediately after cell break-in. Current-clamp recordings were not corrected for a liquid junction potential. Rseries was compensated by bridge balance. Input resistance (Rinput) was monitored using hyperpolarizing current pulses (-50 pA, 200 ms) included in every sweep. Cells were excluded from analysis if Rinput changed by >30%. The membrane time constant (τ) was calculated by single exponential fit of the first 35 ms of the -50 pA current step. Rheobase was defined as the minimum current (500 ms) to elicit at least one spike in 3/6 trials. The current-firing rate relationship (F-I curve) was measured using increasing current injections above rheobase. F-I curves were collected with 5 sweeps per current injection and ISI = 7 s. Spike threshold was defined as the Vm at which the second derivative of Vm was >5 SDs above the prestimulus period, and spike latency was defined as time to spike threshold.

Vm drift correction

Most PV cell recordings for this study were made in current clamp. Accurate measurement of Vm in current clamp experiments is affected by the liquid junction potential, which is typically subtracted from the measured Vm to estimate true Vm. This correction is based on the assumption that the solution interface between internal and cytosol disappears within the first few minutes after patching, creating an offset between measured Vm and true Vm, and that this process is uniform in all cells. For many PV cells, we found that measured resting Vm drifted during the course of a recording. The amount of drift varied, such that uncorrected resting Vm was broadly distributed during the recording epochs when F-I curves and spiking data were being measured. Cell-to-cell variation in resting Vm appeared to be a recording artifact and not true variation in Vm, because both spike threshold and action potential peak covaried with uncorrected resting Vm, with a slope near 1 (**Fig. S1A–B**). The simplest explanation is that differing amounts of drift reflect differing magnitudes of residual liquid junction potential, due to cell-to-cell differences in cytosol replacement by the internal solution. We considered an alternative hypothesis that these were true differences in Vm, which then affected spike threshold or spike peak by regulating the availability of deinactivated Na_V channels or potentially other voltage-activated channels. To test this, we injected tonic current to set resting Vm to approximately -80, -70, or -60 mV, and tested whether this altered spike threshold for spikes elicited by subsequent 500-ms current injection. We found no relationship between manually adjusted resting Vm and spike threshold (**Fig. S1C**). Thus, these experiments did not uncover a causal cell physiological link between uncorrected resting Vm and spike threshold, supporting the interpretation that the covaration between uncorrected resting Vm and spike threshold represents an artifactual offset in Vm measurement. To correct for this artifact, Vm measurements were corrected in each sweep by i) calculating mean measured Vm in the first 5 ms of each sweep, termed “sweep Vm”, and ii) substracting the difference between sweep Vm and the Vrest measured at initial break-in from all Vm values in the sweep. This effectively sets the initial Vm of each sweep to the Vrest break-in value.

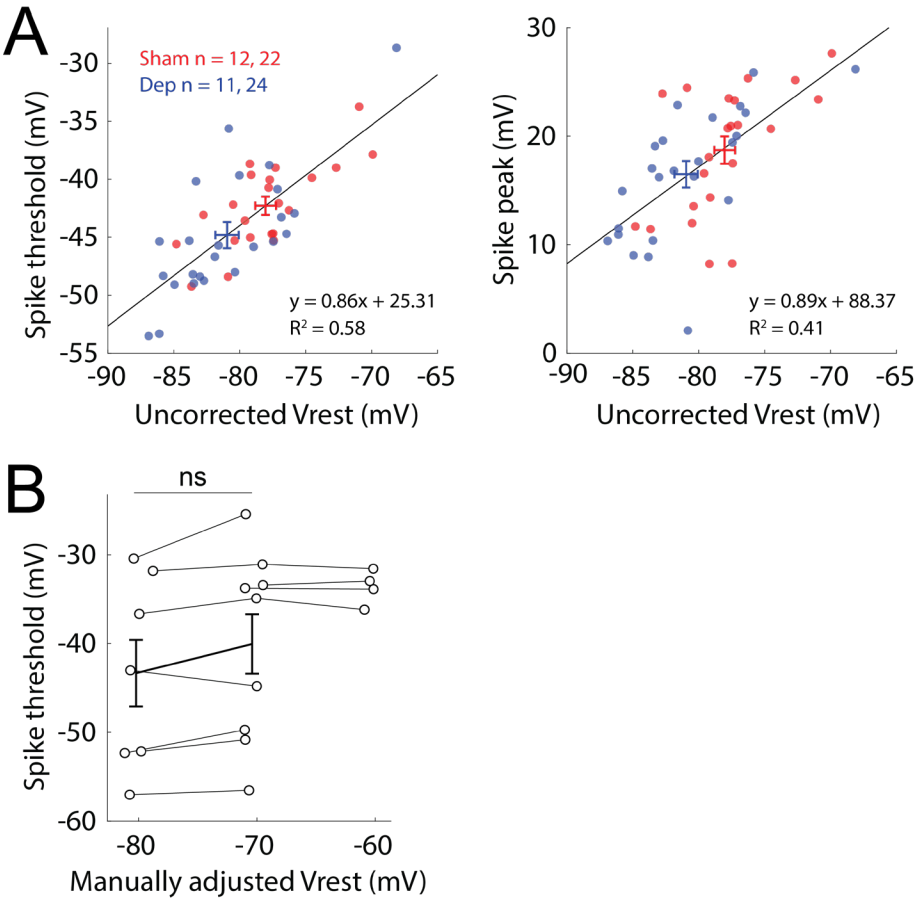

Supplemental Figure S1. Control experiments to test whether uncorrected Vrest values contain an artifactual offset. A, Mean uncorrected Vrest was measured recording of F-I curves and compared to mean spike threshold (left) and mean action potential peak (right). Each dot is one cell. Sham cells (n = 22 cells from 12 mice) are in red and deprived cells (n = 24 cells from 11 mice) are in blue. Ns are given as mice, cells. Regression lines are for all sham and deprived cells combined. **B,** Experimental manipulation of Vrest does not alter spike threshold. We patched L2/3 PV cells and adjusted Vrest by manually changing the holding current. Shown is a within-cell comparison of average spike threshold for F-I curves with Vrest manually adjusted to -80 mV, -70 mV and -60 mV. Connected dots are cells measured at multiple target Vrest values. Average spike threshold was not significantly different when Vrest was adjusted to -80 mV compared to -70 mV ($t_{(6)}$ = -1.84, p = 0.115, paired t test).

L4-evoked synaptic currents

L4-evoked EPSCs and IPSCs were measured in L2/3 PYR cells in whole-cell voltage-clamp mode. All synaptic current measurements were made with the NMDA receptor antagonist D-AP5 in the bath. Rseries was compensated 60%–75%. Cells were discarded from analysis if Rinput was < 100 MΩ. Voltage-clamp recordings were corrected for a 10 mV liquid junction potential. L4 was stimulated with 200 µs constant-current pulses using a bipolar stimulating electrode placed in the center of the barrel that marks the D column (115 µm spacing, FHC). L2/3 PYR cells were recorded from 100–250 µm below the L1-L2/3 boundary and within 100 µm tangentially of the column center. L4-evoked EPSCs and IPSCs were separated by recording at

Vhold = -70 mV and 0 mV (E_{Cl} and E_{AMPA}). Eθ was defined as the minimal stimulus intensity that evoked an EPSC. Input-output curves were collected with 5–7 repetitions of each stimulus intensity and ISI = 10 s. Excitatory and inhibitory synaptic conductances were calculated from measured EPSCs and IPSCs using published methods (Wehr & Zador, 2003; House et al., 2011). Integrated conductance was quantified in a window 3–23 ms after the stimulus.

PV juxtacellular spiking

Juxtacellular recordings were made in PV cells using K-gluconate internal solution. Spiking was recorded in voltage-clamp mode with Vhold manually adjusted to maintain the holding current near 0 pA. Spike probability was calculated over 7–10 sweeps for each L4 stimulus intensity. After recording L4-evoked spiking, we broke into the cell and briefly measured spiking pattern in current-clamp mode to confirm that putative PV cells were fast-spiking.

Experimental design and statistical analysis

D-row deprived and sham mice were littermates, and were recorded interleaved either on the same day or on alternate days. Non-Gaussian data were log-transformed for parametric testing as specified in Results. Reported values are mean ± SEM, except where indicated. 2-tailed tests were used, with $\alpha = 0.05$. Values in the text are mean ± SEM. All statistical tests are identified in the Results. All statistical analyses were performed in Matlab.

3.4 RESULTS

3-day deprivation reduces PV intrinsic excitability

To study deprivation-induced plasticity in L2/3 PV cells in S1, we performed fluorescence-guided whole-cell recordings in S1 slices from PV-cre;tdTomato mice (**Fig. 1A**). We unilaterally plucked the D-row of whiskers for 3 days, beginning at P15–P20, and recorded at P18–P23 (**Fig. 1B**, left). For all experiments, we compared D-deprived mice to age-matched sham-deprived littermates. Recordings were made from PV cells in L2/3 of the D column. To target the D-column, we prepared S1 slices in the "across-row" plane, which allows for visual identification of L4 barrels by transillumination (**Fig. 1B**, right).

To test whether 3 d deprivation decreases the intrinsic excitability of L2/3 PV cells in S1, we performed whole-cell current-clamp recordings of L2/3 PV cells in the presence of glutamate and GABA-A synaptic blockers (in µM: 50 D-AP5, 10 NBQX, and 3 gabazine). We measured F-I curves in PV cells by recording spikes evoked by current injection (500 ms duration) from Vrest. Vrest was not controlled and was allowed to fluctuate freely (with artifactual Vm drift subtracted, see methods and **Fig. S1**). We identified rheobase as the minimum current injection required to produce 1 spike in 3/6 trials. F-I curves were collected in response to set current injections from 0 to 125 pA above rheobase.

Deprivation decreased the slope of F-I curves (n = 22 sham cells from 12 mice, n = 24 deprived cells from 11 mice, $F_{(1,6)} = 9.04$, p = 0.0044, two-way ANOVA, **Fig. 1C,D**). Quantified at 50 pA above rheobase, deprivation reduced spiking from 29.5 ± 1.4 spikes to 23.5 ± 0.9 (mean ± SEM) spikes. Deprivation did not affect latency to the first spike (p = 0.11), or interval between the first and second spike, but interspike interval was reduced for all later spikes ($F_{(1,14)} = 12.4$, p = 0.001, two-way ANOVA, **Fig. 1E**).

Resting and passive properties were largely unchanged. Rheobase was unchanged (p = 0.1822, **Fig. 1F**). Deprivation did not affect resting membrane potential or membrane time constant at rest (p = 0.2807, p = 0.2018). In contrast to the reduction in spiking, deprivation decreased input resistance by 30%, from 54.3 ± 2.8 MΩ in sham cells to 70.4 ± 5.8 MΩ in deprived cells ($t_{(44)} = -2.43$, p = 0.0192, t test, **Fig. 1G**). Sham and deprived groups were age-matched (p = 0.6701), by design. Thus, 3 d deprivation significantly decreased intrinsic the excitability of L2/3 PV cells, despite an increase in input resistance measured near rest.

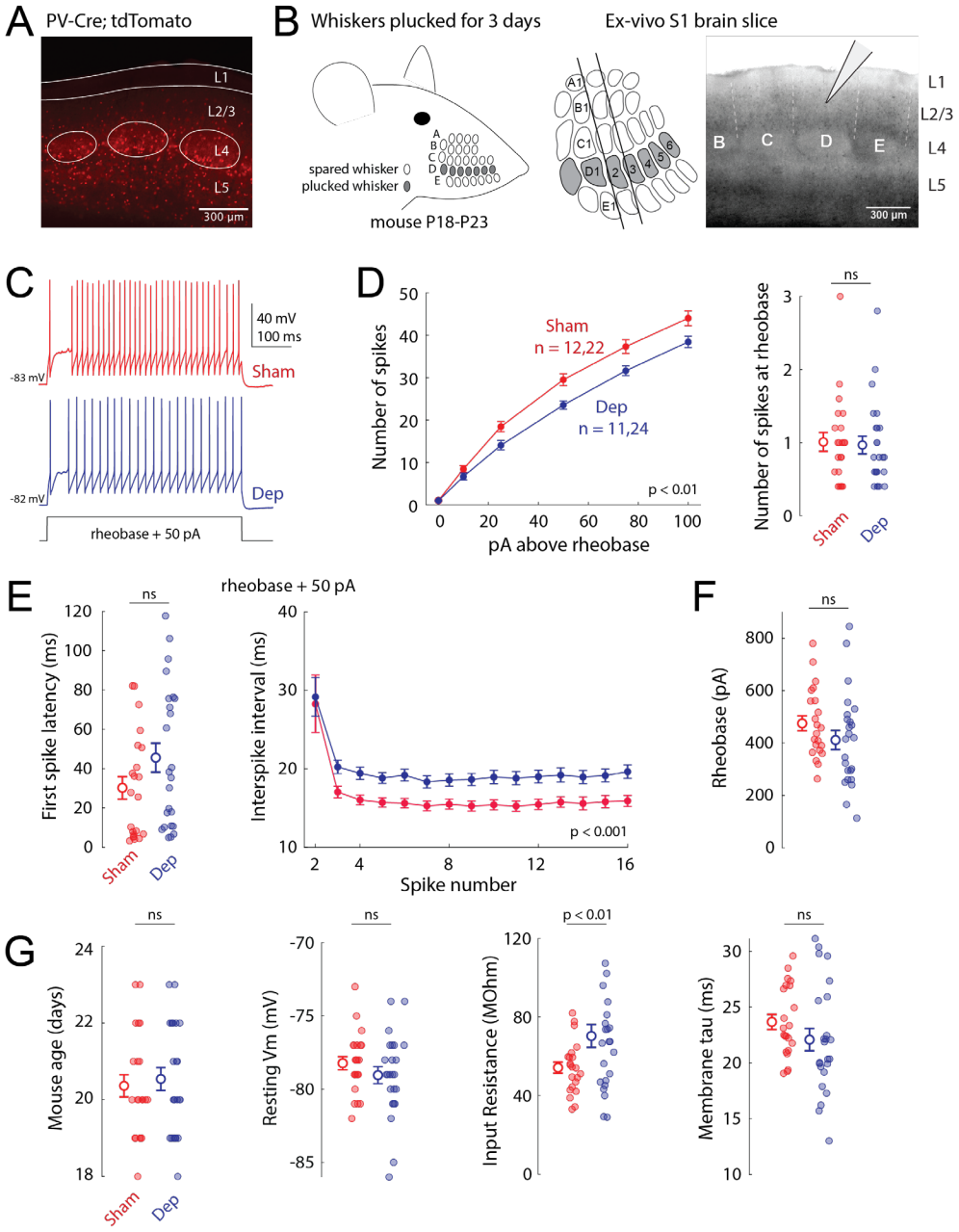

Figure 1. Whisker deprivation decreases intrinsic excitability in L2/3 PV cells. A, Histological section showing fluorescent PV cells in an across-row S1 slice from a PV-Cre;tdTomato mouse, and layer and barrel boundaries estimated from the PV fluorescence pattern. **B,** Schematic of the across-row slice plane, and example transillumination image of a slice as visualized during a recording experiment. The electrode shows the standard location of L2/3 PV recordings in the D column. **C,** Example traces of spiking during F-I curves at rheobase + 50 pA, for a sham and a deprived cell. **D,** Mean F-I curve for 3-day sham and 3-day deprived cells (sham: n = 12 mice, 22 cells, deprived: n = 11 mice, 24 cells). Ns are given as mice, cells. Error bars are SEM, as in all subsequent figures. P-value is deprivation factor in a 2-way repeated measures ANOVA. Right, the number of spikes elicited at rheobase was unchanged by deprivation, demonstrating consistency in identifying rheobase between spared and deprived cells. **E,** Left, Latency to first spike measured at 50 pA above rheobase. ($t_{(44)}$ = -1.63, p=0.11, t-test). Right, interspike interval preceding each spike at 50 pA above rheobase. **F,** Rheobase for each cell. **G,** Mouse age and passive properties for each cell.

Reduced excitability is associated with changes in the AHP, not spike threshold

We next tested whether changes in the afterhyperpolarization (AHP) or spike threshold underlie the decrease in intrinsic excitability in L2/3 PV cells. We calculated the mean waveform of the spike plus subsequent AHP, for all spikes evoked at rheobase + 10 pA. Analysis was restricted to spikes with a pre-spike Vm between -50 mV and -43 mV, to ensure similar starting conditions before the spike. This revealed that 3 d whisker deprivation increased the average depth of the medium afterhyperpolarization (mAHP) (**Fig. 2A**, left). To prevent subsequent spikes from contaminating AHP dynamics, we further limited analysis to spikes for which the subsequent ISI was > 50 ms (**Fig. 2A**, right). We quantified mAHP depth 25 ms after spike onset and found that mAHP depth was 1.7 ± 0.4 mV in sham-deprived cells, and that this increased to 3.6 ± 0.7 mV in deprived cells ($t_{(39)}$= -2.37, p = 0.0204, t test, **Fig. 2A**). In contrast, 3 d deprivation did not affect spike threshold ($F_{(1,10)}$ = 0.024, p = 0.8777, two-way ANOVA, **Fig. 2B**). This contrasts with previous work that found 1 d deprivation increases spike threshold in L2/3 PV cells (Gainey et al., 2018).

3-day deprivation also decreased the depth of the fast afterhyperpolarization (fAHP) measured 1–1.5 ms after spike onset ($t_{(44)}$ = 2.81, p = 0.0073, t test, **Fig. 2C,D**). Action potential height and width were not significantly different for sham and deprived cells ($t_{(44)}$ = -3.6, p = 0.7208, $t_{(44)}$ = -1.74, p = 0.0897, **Fig. 2D**). Thus, 3 d D-row deprivation prolongs or strengthens the mAHP without affecting spike threshold, suggesting that 3 d deprivation reduces PV spiking by a different mechanism than that for 1 d deprivation.

3-day deprivation does not change L4-evoked feedforward excitation or inhibition in L2/3 PYR cells

Decreased excitability of L2/3 PV cells could result in a decrease in feedforward L4–L2/3 inhibition, which is primarily mediated by PV cells. To test whether deprivation alters feedforward inhibition or excitation, we studied L4-evoked excitation and inhibition onto L2/3 PYR cells. We electrically stimulated in L4 and measured evoked EPSCs and IPSCs in L2/3 PYR cells in the D column (**Fig. 3A**). EPSCs and IPSCs were separated in voltage clamp by recording at -70 and 0 mV (E_{Cl} and E_{AMPA}). Previous work found that L4 stimulation recruited feedforward, disynaptic inhibition with modest contamination from monosynaptic inhibition (Gainey et al., 2018). NMDA receptors were blocked with D-AP5 (50 μM) in all experiments. For each L2/3 PYR cell, we found the minimum stimulation intensity that elicited an EPSC (termed Eθ) and measured EPSCs and IPSCs in input-output curves from 1.0–1.4 x Eθ. Currents were integrated over the first 20 ms for analysis. Surprisingly, deprivation did not significantly affect input-output curves for Gex or Gin (n = 37 sham cells from 16 mice, n = 35 deprived cells from 17 mice, Gex: $F_{(1,4)}$ = 2.24, p = 0.1394, Gin: $F_{(1,4)}$ = 1.38, p = 0.2443, two-way ANOVA on log-transformed data, **Fig. 3B**). If anything, there was a trend toward increased Gex, but this was not significant.

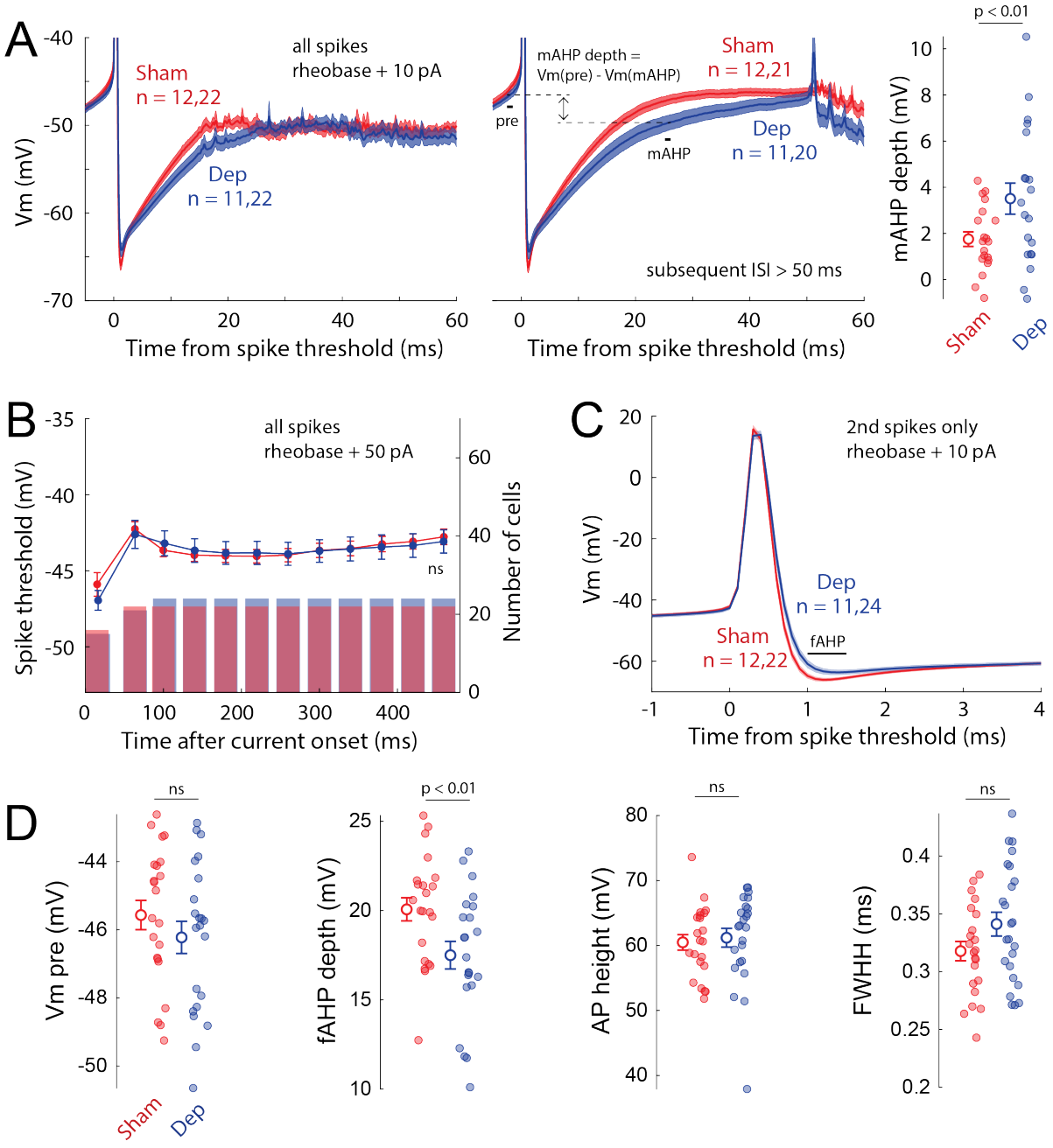

Figure 2. Whisker deprivation strengthens mAHP in L2/3 PV cells **A,** Average mAHP for sham and deprived cells (sham: n = 12 mice, 22 cells; deprived: n = 11 mice, 22 cells). Left, mean mAHP traces for all spikes at 10 pA above rheobase (sham: n = 12 mice, 22 cells; deprived: n = 11 mice, 22 cells). Center, mAHPs for spikes with a subsequent ISI > 50 ms. Right, mean mAHP depth measured 25–26 ms after spike threshold crossing. Shaded regions and bars are the SEM. **B,** Mean spike threshold for all spikes recorded at 50 pA above rheobase, in 40 ms time bins starting from current onset. Bars indicate number of cells for each time bin. **C,** Mean shape of second spike at 10 pA above rheobase, across all sham and deprived cells (sham: n = 12 mice, 22 cells; deprived: n = 11 mice, 22 cells). **D,** Quantification of spike shape for spikes in **C**. Pre-spike Vm did not differ for sham and deprived groups. The p values are from two-tailed t tests.

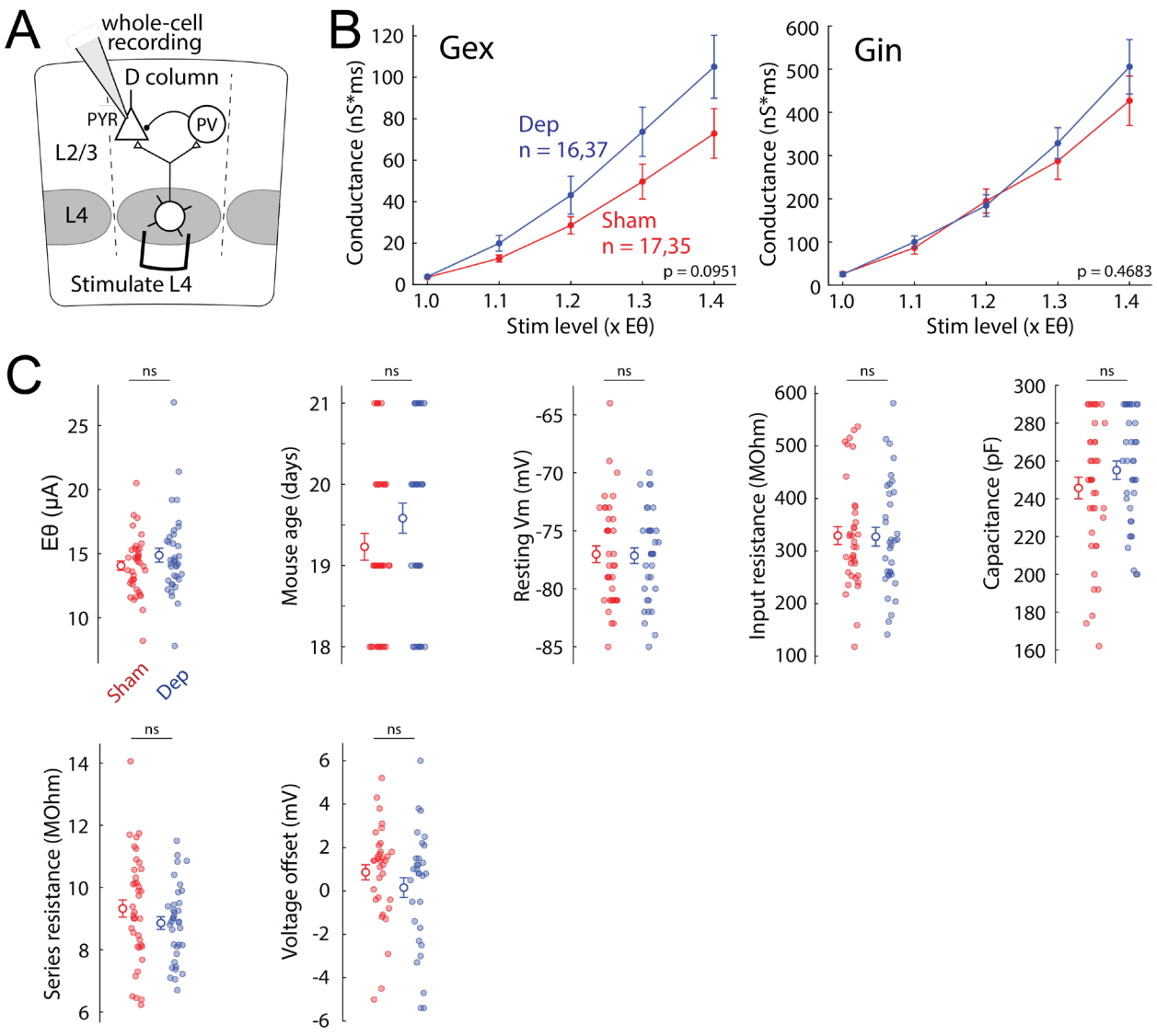

Figure 3. 3-day deprivation does not change L4-evoked conductances in L2/3 PYR cells. A, Schematic of L4 electrical stimulation and whole-cell recordings in L2/3, showing circuit for L4–L2/3 feedforward excitation and inhibition. **B,** Mean input-output curves for integrated Gex and Gin with increasing L4 stimulation intensity (sham: n = 35 cells from 17 mice; deprived: 37 cells from 16 mice). Error bars are SEM. P-values are for deprivation factor in a 2-way repeated measures ANOVA on log-transformed data. **C,** Sham and deprived groups did not differ in Eθ, mouse age, or passive properties.

Eθ was not affected by deprivation, indicating similar stimulation efficacy for sham and deprived groups ($t_{(73)} = -1.42$, p = 0.1584, t test, **Fig. 3C**). Sham and deprived groups were age-matched by design and did not differ in passive properties (**Fig. 3C**). Deprivation did not affect the offset potential measured after removing the electrode from the cell at the end of each recording (**Fig. 3C**). Thus, 3 day deprivation does not reduce L4-evoked conductances in L2/3 PYR cells, despite a decrease in the excitability of L2/3 PV cells.

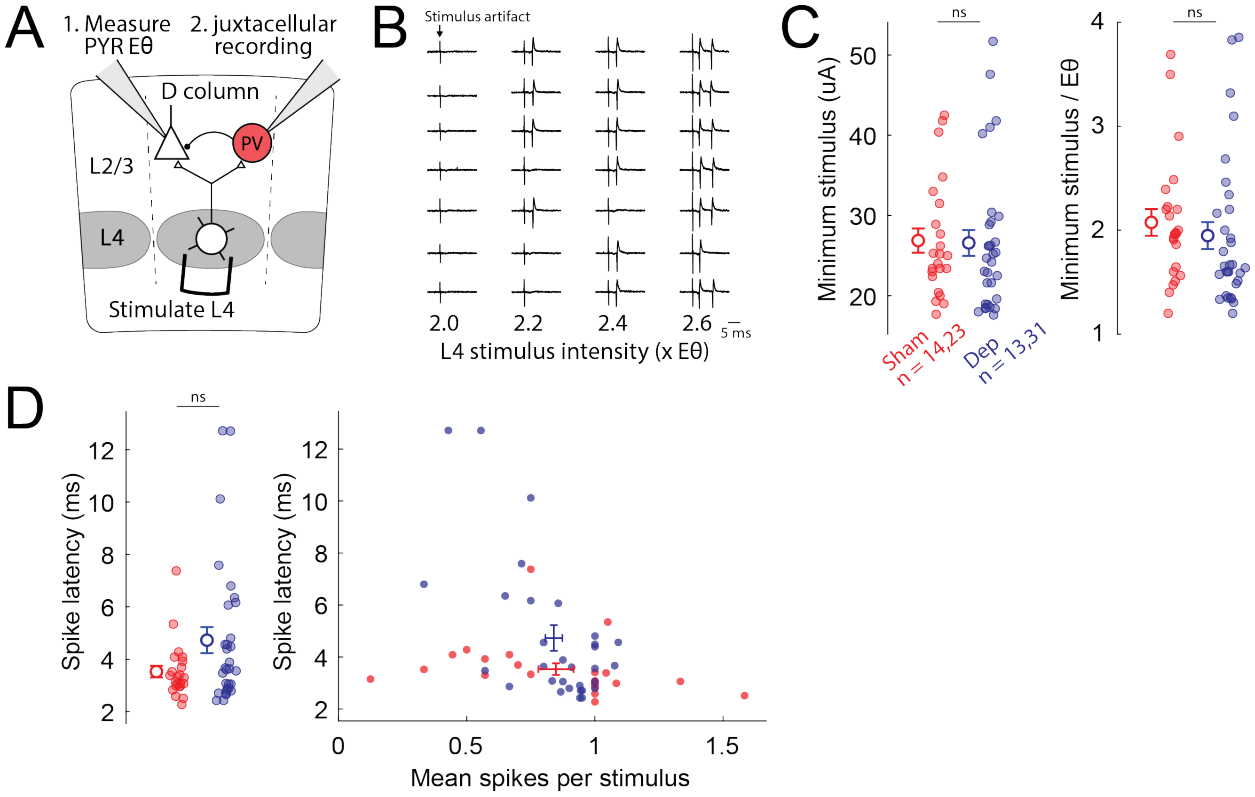

Figure 4. 3-day deprivation does not change L4-evoked spiking in PV neurons. A, Schematic of L4-evoked spiking in L2/3 PV cells. EΘ was measured for 1–2 L2/3 PYR cells, then L4-evoked spikes were recorded for PV cells in the same column. **B,** Example spike traces from one cell across multiple stimulation intensities. **C,** Left, minimum stimulus intensity that evoked spikes in sham and deprived PV cells (sham: n = 14 mice, 23 cells, deprived: n = 13 mice, 31 cells). Right, measurements on left divided by average EΘ for PYR cells in the same column. **D,** Left, latency to first spike, measured at minimum stimulus intensity. Data were log-transformed before t test. Right, within-cell comparison of spike latency and average number of evoked spikes. Each point is a cell.

3-day deprivation does not change L4-evoked spiking in PV cells

To understand why L4-evoked inhibition was not altered by deprivation, we next tested whether 3 day deprivation affected L4-evoked spiking in PV cells. We performed 3 day whisker deprivation in PV-cre;tdTomato mice, made S1 slices, and electrically stimulated in L4 of the D column, as in the prior experiments. In each slice, we first performed whole-cell voltage clamp recordings from 1–2 L2/3 PYR cells in the D column, and determined EΘ as in the prior experiment. Then, we made cell-attached recordings from L2/3 PV cells in the same column, and measured juxtacellular spikes evoked by L4 stimulation. We varied L4 stimulation intensities between 1.0–5.0 x EΘ in order to find the stimulus threshold required to evoke a single spike from the PV cell. Our hypothesis was that if PV cells are less excitable, stronger L4 stimulus intensity should be required to synaptically evoke a L2/3 PV spike.

We quantified L4-evoked spiking in 23 sham PV cells from 14 mice and 31 deprived PV cells from 13 mice. Deprivation did not change the minimal stimulus intensity required to evoke spiking in PV cells ($t_{(52)}$ = 0.13, p = 0.8969, t test, **Fig. 4C**, left). In agreement with previous findings, most PV cells were not recruited to spike within the range of stimulus intensities used to measure L4-evoked Gex and Gin in L2/3 PYR cells (Gainey et al., 2018). For spikes evoked at the minimum stimulus level, we quantified first spike latency relative to L4 stimulation. Sham and deprived cells did not differ in the mean latency to first spike, with a small trend toward longer latency in deprived cells ($t_{(52)}$ = -1.94, p = 0.0584, t test on log-transformed data, **Fig. 4D**). Deprivation did not affect the mean number of spikes evoked at the minimum stimulus level. (**Fig. 4D**, right). Thus, we found no evidence that 3-day deprivation changed the L4-evoked spiking of L2/3 PV cells. This may be expected, since L4 stimulation evokes only brief activation of PV cells (Gainey et al., 2018), and PV intrinsic excitability was only reduced by deprivation for late spikes, not the first 1–2 spikes (**Fig. 1**).

1-day deprivation does not decrease PV intrinsic excitability

We sought to confirm previous findings that that 1 day whisker deprivation decreases the intrinsic excitability of L2/3 PV cells in S1 (Gainey et al., 2018). As described for 3-day deprivation experiments, we performed fluorescence-guided recordings in PV-cre;tdTomato mice. We unilaterally plucked the D-row of whiskers for 1 day, beginning at P17–P21, and recorded at P18–P22. We compared 1-day D-deprived mice to age-matched, sham-deprived littermates. We prepared across-row slices and recorded from PV cells in L2/3 of the D column.

To test the effects of 1 d deprivation on PV cell intrinsic excitability, we performed whole-cell current-clamp recordings of L2/3 PV cells as described for 3-day deprivation experiments. **Figure 5A** shows example traces from sham and deprived cells at 50 pA above rheobase. Surprisingly, 1-day deprivation did not change the slope of F-I curves (n = 28 sham cells from 11 mice, n = 24 deprived cells from 9 mice, $F_{(1,6)}$ = 4.46, p = 0.5072, two-way ANOVA, **Fig. 5B**). Measured at 50 pA above rheobase, sham cells had 28.4 ± 1.1 spikes compared to 27.3 ± 1.5 (mean ± SEM) spikes in deprived cells. Deprivation did not affect latency to the first spike ($t_{(50)}$ = 0.58, p = 0.5652, **Fig 5C**, left). Whereas 3-day deprivation shortened the preceding interspike interval for all but the first two spikes, 1 day deprivation had no effect on interspike interval across all spikes ($F_{(1,14)}$ = 3.62, p = 0.55, two-way ANOVA, **Fig. 5C**, right).

Sham and deprived cells did not differ in passive properties. Rheobase was not changed by deprivation ($t_{(50)}$ = 0.03, p = 0.9705, t test, **Fig. 5D**). Deprivation did not affect resting membrane potential or membrane time constant at rest ($t_{(50)}$ = -1.38, p = 0.1727, $t_{(50)}$ = -0.73, p = 0.4652). In contrast to the strong reduction in input resistance for 3 day deprivation, 1 day deprivation did not affect input resistance ($t_{(50)}$ = 0.63, p = 0.5299, **Fig. 5E**). Sham and deprived groups were age-matched ($t_{(50)}$ = -0.44, p = 0.6622), by design. Thus, in contrast with previous findings, 1 d deprivation did not affect the spiking excitability of L2/3 PV cells.

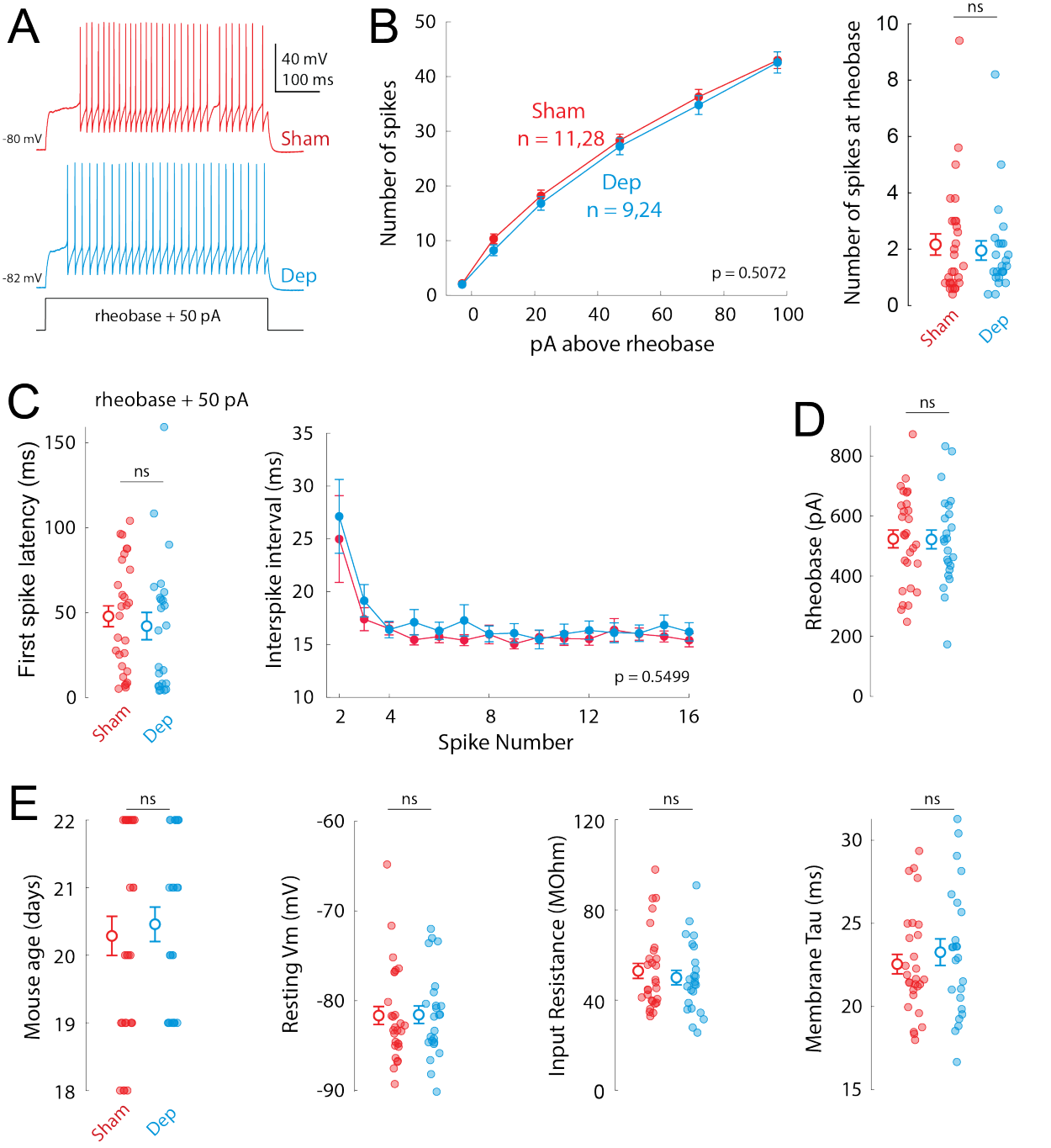

Figure 5. 1-day deprivation does not decrease intrinsic excitability in L2/3 PV cells. A, Example traces of spiking during F-I curves at rheobase + 50 pA, for a sham cell and a deprived cell. **B,** Left, mean F-I curve for 1-day sham and 1-day deprived cells (sham: n = 28 cells from 11 mice; deprived: n = 24 cells from 9 mice). P-value is deprivation factor in a two-way repeated measures ANOVA. Right, the number of spikes elicited at rheobase was unchanged by 1 d deprivation. **C,** Left, first spike latency measured at 50 pA above rheobase. ($t_{(50)}$ = 0.58, p = 0.6798, t test). Right, interspike interval preceding each spike at 50 pA above rheobase. **D,** Rheobase for each cell. **E,** Mouse age and passive properties for each cell.

1-day deprivation does not drive changes in the AHP or spike threshold

We next looked beyond spike number, to test whether 1 day deprivation affected AHPs, spike threshold, or spike shape. We analyzed 1 day spiking data as described for our 3 day deprivation experiments in **Figure 2**. We computed the average waveforms for spikes evoked at 10 pA above rheobase and restricted pre-spike Vm to between -50 mV and -43 mV. Unlike 3 day deprivation, 1 d whisker deprivation did not change the average depth of the mAHP (**Fig. 6A**, left). Nor was there a difference between sham and deprived waveforms when we restricted analysis to spikes having a subsequent ISI > 50 ms (**Fig. 6A**, right). Mean mAHP depth quantified 25 ms after spike onset was 4.9 ± 0.5 mV in sham cells and 5.6 ± 0.6 mV in deprived cells ($t_{(39)}$ = -0.80, p = 0.4289, t test, **Fig. 6A**, right). Deprivation did not affect spike threshold ($F_{(1,10)}$ = 0.13, p = 0.7226, two-way ANOVA, **Fig. 6B**). While this result contrasts with the previous finding that 1 d deprivation increases spike threshold (Gainey et al., 2018), is consistent with 1 day deprivation having no effect on the number of spikes evoked by current injection.

We also quantified spike shape for 1 day whisker deprivation. There was no change in the depth of the fAHP measured 1–1.5 ms after spike onset ($t_{(44)}$ = 2.81, p = 0.0073, t test, **Fig. 6C,D**). Action potential height and width were not significantly different for sham and deprived cells ($t_{(44)}$ = -0.41, p = 0.6808, $t_{(50)}$ = 1.57, p = 0.1233, **Fig. 6D**). Thus, we found no evidence for changes in mAHP, fAHP, spike shape or spike threshold following 1 d D-row whisker deprivation. These results indicate that mAHP changes in PV cells require 3 days of deprivation to occur, and do not occur at 1 day of deprivation.

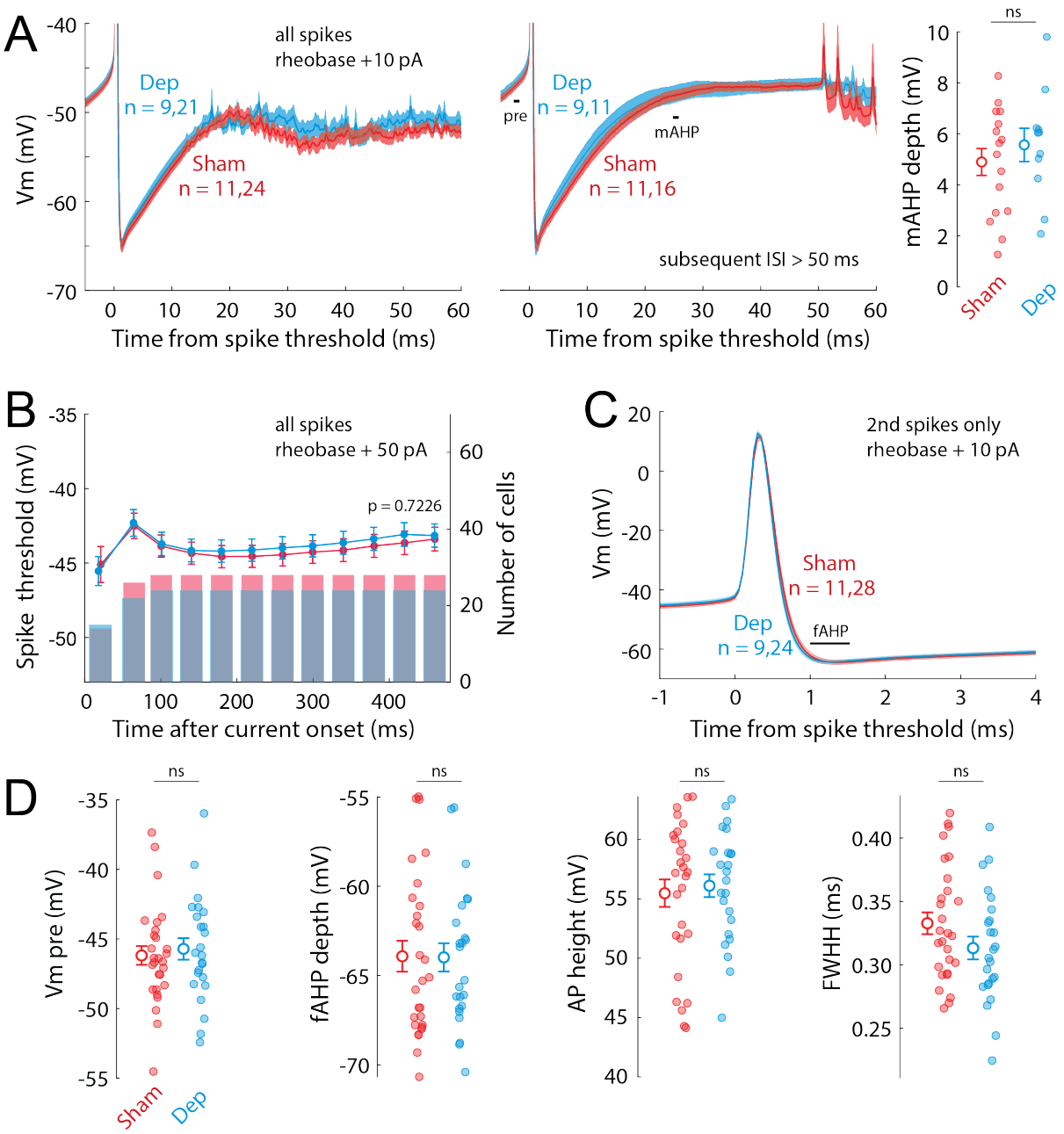

Figure 6. 1-day deprivation does not strengthen the mAHP in L2/3 PV cells. A, Average mAHP for sham and deprived cells (sham: n = 11 mice, 24 cells; deprived: n = 9 mice, 21 cells). Left, mean mAHP traces for all spikes at 10 pA above rheobase (sham: n = 11 mice, 16 cells; deprived: n = 9 mice, 11 cells). Center, mAHPs for spikes with a subsequent ISI > 50 ms. Right, mean mAHP depth measured 25–26 ms after spike threshold crossing. Shaded regions and bars are the SEM. **B,** Mean spike threshold for all spikes recorded at 50 pA above rheobase, in 40 ms time bins. Bars are number of cells per time bin. **C,** Mean shape of second spikes at 10 pA above rheobase, for all sham and deprived cells (sham: n = 11 mice, 28 cells; deprived: n = 9 mice, 24 cells). **D,** Quantification of spike shape for spikes in **C**. There was no difference in pre-spike Vm for sham and deprived cells. The p values are for two-tailed t tests.

3.5 DISCUSSION

Neurons can change their intrinsic excitability in a variety of ways, including changes in resting membrane potential, spike threshold, and input resistance. We show that PV neurons in S1 can adjust their intrinsic excitability in two distinct ways: In previous work, brief 1-day deprivation decreased PV spiking excitability through an increase spike threshold (Gainey et al., 2018). In this study, we find that that 3-day deprivation strengthens or prolongs the mAHP without affecting spike threshold. Thus, different time scales of whisker deprivation recruit distinct plasticity mechanisms in L2/3 PV neurons.

Whisker map plasticity in S1

This study advances our understanding of how PV inhibitory circuits change during map plasticity in S1. In classical whisker map plasticity, prolonged deprivation (>5 days) of a row of whiskers weakens the whisker-evoked spiking for those whiskers in L2/3, thus reducing the representation of deprived whiskers in the somatotopic whisker map (Feldman, 2009). This process involves LTD at feedforward L4 excitatory synapses onto L2/3 pyramidal cells in deprived whisker columns (Allen et al., 2003; Bender, Allen, Bender, & Feldman, 2006; L. Li et al., 2009). Because LTD is a rapid plasticity process that can be induced in minutes, it was initially unclear why shorter durations of whisker deprivation do not drive depression of whisker-evoked spiking in cortex – indeed, brief periods of deprivation in rat either stabilize (1 day) or slightly increase (3 days) whisker-evoked spiking in L2/3 PYRs, rather than depressing it (L. Li et al., 2014). The answer was apparent from examining whisker-evoked EPSCs and IPSCs in L2/3 PYR cells *in vivo*, which revealed that 3-day deprivation decreases whisker-evoked EPSCs in L2/3 PYRs measured *in vivo*, consistent with Hebbian weakening of excitatory inputs, but weakens whisker-evoked IPSCs even further, increasing whisker-evoked E-I ratio. This stabilizes net synaptic drive to L2/3 PYRs (L. Li et al., 2014). These observations suggest that disinhibition is an active homeostatic process that occurs rapidly and offsets the loss of whisker-evoked excitation in order to stabilize whisker-evoked firing in L2/3. The cellular mechanisms for rapid weakening of inhibition were localized to L2/3 PV neurons, where deprivation causes a rapid decrease in L2/3 PV intrinsic excitability in mice (Gainey et al., 2018). 1-day deprivation was shown to decrease F-I curves in L2/3 PV cells, without detectable changes in L4 excitatory synapse strength onto PV cells or PV inhibitory synapse strength onto L2/3 PYR cells (Gainey et al., 2018). Thus, 1-day deprivation was known to drive a reduction in L2/3 PV intrinsic excitability, leading to reduced feedforward PV-mediated disinhibition in deprived columns. This phenomenon was termed ‘PV circuit homeostasis’ and was proposed stabilize L2/3 PYR firing rates in response to naturally varying levels of whisker input (Gainey et al., 2018).

The conceptual question behind the current study was to determine whether the cellular mechanisms of PV circuit homeostasis are stable or change with longer durations of whisker deprivation. Existing studies do not paint a clear picture of how mechanisms change with deprivation duration, because some studies have used rats and others mice. In rats, deprivation weakens whisker-evoked IPSCs in L2/3 PYR cells after 3 days of deprivation,

continuing at least through 10 days of deprivation (L. Li et al., 2014). Cellular mechanisms have only been examined at >5 days of deprivation, and involve weakening of L4 excitation onto L2/3 PV neurons, with no change in PV intrinsic excitability (House et al., 2011). L2/3 recurrent inhibition is also reduced, suggesting decreased L2/3 PYR excitatory input onto PV cells (Shao et al., 2013). In mice, 1 day of deprivation is sufficient to weaken PV inhibition, and this early phase of PV circuit homeostasis involves a reduction in PV intrinsic excitability without any measurable change in L4–L2/3 excitatory input onto PV cells (Gainey et al., 2018). If mechanisms are assumed to be identical in mice and rats, then rapid PV disinhibition in S1 appears to begin with a reduction in PV intrinsic excitability, with longer deprivation driving synaptic changes in PV circuits.

The cellular mechanisms of PV circuit plasticity may also differ between cortical areas. A similar rapid decrease in PV inhibition is observed in binocular V1 where 1 day of monocular deprivation reduces visually evoked spiking of L2/3 PV neurons, causing an increase in the firing of L2/3 PYR cells (Kuhlman et al., 2013). However, the implementation of rapid PV plasticity appears to be different in V1, since monocular deprivation rapidly reduces L4 and L5a excitatory synaptic strength onto L2/3 PV neurons in mice (Kuhlman et al., 2013), an effect that doesn't occur in S1 until > 5 days of deprivation in rats (House et al., 2011). Thus, brief, 1-day sensory deprivation drives weakening of L2/3 PV circuit function in S1 via changes in PV intrinsic excitability, but in V1 via synaptic weakening within PV circuits.

Our results show that 3-day deprivation reduces spiking excitability in L2/3 PV neurons, measured as a decrease in F-I curves (**Fig. 1**), and that this is caused not by a change in spike threshold (**Fig. 2**), but by a deepening and lengthening of the mAHP that sets the interval between spikes (**Fig. 2**). We did not detect a change in L4 excitation onto PV cells (**Fig. 3**). Thus, 3-day deprivation was similar to the prior reported findings for 1-day deprivation in affecting PV intrinsic excitability, rather than L4-evoked excitatory input. However, the specific mechanisms for reduced intrinsic excitability differed at these two time points, with 3-day deprivation affecting mAHPs but not spike threshold.

Mechanisms underlying the reduction in intrinsic excitability with 3-day deprivation

Our results suggest that PV spiking is reduced after 3-day deprivation through a different mechanism than reported previously for 1-day deprivation. Unlike 1-day deprivation, 3-day deprivation does not change spike threshold (**Fig. 2B**) and increases input resistance at rest (**Fig. 1G**). Changes in a wide array of conductances are known to affect intrinsic excitability (Zhang & Linden, 2003). Intrinsic excitability can also be regulated by the subcellular localization of ion channels, including changes in the length and location of the axon-initial-segment (AIS) (Grubb & Burrone, 2010; Jamann et al., 2021).

Previous work showed that 1-day deprivation increases near-threshold excitability in part by upregulating Kv1 currents (Gainey et al., 2018). Low-threshold Kv1 delayed rectifier channels are a key determinant of spike threshold and excitability in L2/3 PV neurons (Goldberg et al.,

2008). In hippocampal PV basket cells, synaptic stimulation downregulates Kv1.1 and increases intrinsic excitability—this process requires activation of metabotropic glutamate receptor subtype 5 (mGluR5) and mammalian target of rapamycin complex 1 (mTORC1) (Campanac et al., 2013; Khlaifia, Honoré, Artinian, Laplante, & Lacaille, 2022). Kv1 channels also regulate PV excitability in S1, where L2/3 PV cells with greater Kv1.1 expression have lower spike threshold and a longer latency to first spike after current injection (Dehorter et al., 2015).

Recent studies have identified signaling pathways that could regulate PV excitability through changes in Kv1 current. In L2/3 of S1, PV cells that strongly express the transcription factor Er81 are less excitable, exhibiting a characteristic delayed firing pattern (Dehorter et al., 2015). Moreover, artificial manipulations of network activity drive bidirectional changes in Er81 levels and PV spiking, making Er81 a compelling candidate for rapid plasticity of PV intrinsic excitability (Dehorter et al., 2015). Kv1 channels are also regulated through neuregulin-1 (NRG1) signaling via the tyrosine kinase receptor ErbB4 (K.-X. Li et al., 2012). NRG1/ErbB4 signaling increases the intrinsic excitability of PV neurons by downregulating Kv1.1, causing a decrease in spike threshold. Interestingly, decreased NRG1/ErbB4 signaling is necessary for rapid weakening of PV circuits in V1 following 1-day monocular deprivation, though NRG1 treatment does not alter the intrinsic excitability of V1 PV cells (Y. Sun et al., 2016).

Previous work also showed that A-type K currents in PV cells are upregulated by 1-day D-row deprivation (Gainey et al., 2018). A-type currents are rapidly inactivating and predominantly mediated by Kv1.4 and Kv4 channels (Gutman et al., 2005). The role of A-type currents in PV neuron plasticity is largely unknown. Sustained (3 week) whisker deprivation increases A-type currents in L4 PV neurons and increases spiking excitability (Q.-Q. Sun, 2009). This is associated with an increase in action potential threshold and a decrease in input resistance at rest (Q.-Q. Sun, 2009).

PV cell excitability could also be regulated though Kv3 channels, which facilitate rapid action potential repolarization in PV neurons and enable the 'fast-spiking' phenotype (Du, Zhang, Weiser, Rudy, & McBain, 1996; Lau et al., 2000; Rudy & McBain, 2001). Kv3 channels have a high voltage threshold for activation (>-20 mV) and a rapid deactivation rate, suggesting that they could regulate spike rate without influencing spike threshold (Gutman et al., 2005). Relatively little is known about K_V3 regulation in interneurons. In visual cortex, PV cell maturation during the critical period coincides an increase in Kv3.1 expression (Du et al., 1996); more recent work shows that Kv3.1 expression in PV neurons influences the rate of critical period ocular dominance plasticity (Matsuda, Miyamoto, Joho, & Hensch, 2021). Additionally, experimental activation of TrkB receptors on PV neurons regulates network plasticity in part by regulation of Kv3 currents in PV neurons (Winkel et al., 2021).

Another potential regulator of PV cell firing is the hyperpolarization-activated cyclic nucleotide-gated (HCN) channel. Neuronal HCN channels are regulated by activity and can influence excitability in complex ways (Fan et al., 2005; Shah, 2014). A recent study in rat hippocampal PV basket cells found that axon-specific HCN channel expression enhances AP initiation and

facilitates high-frequency firing (Roth & Hu, 2020). Thus, a deprivation-driven decrease in HCN expression could explain both a decrease in PV spiking and our observed increase in input resistance at rest.

Lack of network effect for 3-day deprivation

Although 3-day deprivation decreased PV spiking excitability, we were unable to detect network-level changes in inhibition after 3-day deprivation. We saw no change in L4-evoked PV spiking or in L4-evoked feedforward inhibition in L2/3 PYR neurons (**Figs. 3-4**). One explanation for this apparent discrepancy is that 3-day deprivation only reduced excitability in the context of sustained firing. This is supported by our measurements of spike latency, where there was no change in the latency to the first spike or the interval between the first and second spike; rather, interspike interval was only reduced for later spikes (**Fig. 1E**). We hypothesize that L4 evoked PV spiking was unchanged because L4 stimulation only evoked 1–2 action potentials in PV neurons. Thus, PV neurons were not in the sustained-firing regime in which we would expect 3-day deprivation to reduce spike rate.

Failure to replicate 1-day deprivation effects

As part of the current study, we attempted to replicate the previously reported effect that 1-day deprivation reduces PV intrinsic excitability, and does so by increasing spike threshold (Gainey et al., 2018). Surprisingly, we did not observe any decrease in F-I curves with 1-day deprivation (**Fig. 6**). Instead, 1-day deprivation did not drive any significant changes in PV cell spiking or in passive properties. We attempted to replicate as many conditions as possible from the prior study. Both studies used the same mouse strain (PV-Cre;tdTomato or C57Bl/6, The Jackson Laboratory #000664), at the same age, and combined both males and females. Both studies used the same method of whisker deprivation (plucking under brief isoflurane anesthesia). In both studies, the same slice method was used and the D column was localized by the same method. It is possible that slices were prepared at systematically different times in the mouse's light cycle, or that individual differences in whole-cell patching methods led to somewhat different intracellular conditions in the two studies. We do not know what factors were responsible for the different results at 1 day of deprivation. However, our positive findings of mAHP changes at 3 days of deprivation demonstrate a novel cellular mechanism for plasticity of PV intrinsic excitability.

Effect of 3-day deprivation on PV circuit function *in vivo*

How might 3-day deprivation affect PV neuron activity *in vivo*? Since spike latency was reduced only when PV cells fired multiple spikes, we hypothesize that 3-day deprivation selectively reduces firing rate when PV cells fire at a high frequency. In S1, PV neurons can fire rapidly in response to sensory stimuli: recent work showed that whisker touch elicits multiple spikes in L2/3 PV-expressing fast-spiking interneurons, with average touch-evoked spike count of 2.0 spikes per touch at firing rates exceeding 100 Hz, and multiple touches per whisking bout (Yu,

Hu, Agmon, & Svoboda, 2019). Thus, while 3-day deprivation did not affect L4-evoked PV spiking *in vitro*, we hypothesize that deprivation could nonetheless suppress PV firing rates during periods of rapid sensory-driven activity.

Rapid PV firing is also a key component of cortical gamma oscillations (30–90 Hz), which temporally coordinate sensory information and support perception (Buzsáki & Wang, 2012; Cardin et al., 2009). Recent work shows that a subset of PV neurons in S1 fire regularly at gamma frequencies, independent of sensory input (Shin & Moore, 2019). Thus, by reducing PV firing at gamma frequencies, we speculate that whisker deprivation could suppress gamma oscillations in S1. Indeed, previous work shows that long-term (~7 day) whisker deprivation decreases gamma-band activity and reduces recurrent inhibition in L2/3 of S1 (Shao et al., 2013).

This study demonstrates that the cellular mechanisms of PV circuit homeostasis change with longer durations of whisker deprivation. Brief (1-day) deprivation decreases PV spiking excitability through an increase spike threshold (Gainey et al., 2018), while longer (3-day) deprivation strengthens the mAHP. Sustained deprivation (>5 days) drives changes in L4 synaptic input (House et al., 2011). This differs from PV circuit plasticity in V1, where excitatory inputs to L2/3 PV neurons weaken in as little as 1 day (Kuhlman et al., 2013). Thus, the mechanisms for experience-dependent plasticity of cortical inhibitory circuits differ over time and between cortical regions. This study also shows that the mAHP in PV cells is regulated by activity—we predict that distinct cellular mechanisms underlie this plasticity. Although we were unable to detect network-level changes in inhibition after 3-day deprivation, we predict that that 3-day deprivation selectively reduces PV firing rates when PV cells fire at a high frequency .

3.6 ACKNOWLEDGEMENTS

J.W.A was supported by a NSF Graduate Research Fellowship (DGE 1752814).

3.7 REFERENCES

Allen, C. B., Celikel, T., & Feldman, D. E. (2003). Long-term depression induced by sensory deprivation during cortical map plasticity in vivo. *Nature Neuroscience*, *6*, 291–299.

Atallah, B. V., Bruns, W., Carandini, M., & Scanziani, M. (2012). Parvalbumin-Expressing Interneurons Linearly Transform Cortical Responses to Visual Stimuli. *Neuron*, *73*, 159–170.

Avermann, M., Tomm, C., Mateo, C., Gerstner, W., & Petersen, C. C. H. (2012). Microcircuits of excitatory and inhibitory neurons in layer 2/3 of mouse barrel cortex. *Journal of Neurophysiology*, *107*, 3116–3134.

Barnes, S. J., Sammons, R. P., Jacobsen, R. I., Mackie, J., Keller, G. B., & Keck, T. (2015). Subnetwork-Specific Homeostatic Plasticity in Mouse Visual Cortex In Vivo. *Neuron*, *86*, 1290–1303.

Bender, K. J., Allen, C. B., Bender, V. A., & Feldman, D. E. (2006). Synaptic basis for whisker deprivation-induced synaptic depression in rat somatosensory cortex. *The Journal of Neuroscience: The Official Journal of the Society for Neuroscience*, *26*, 4155–4165.

Buzsáki, G., & Wang, X.-J. (2012). Mechanisms of Gamma Oscillations. *Annual Review of Neuroscience*, *35*, 203–225.

Campanac, E., Gasselin, C., Baude, A., Rama, S., Ankri, N., & Debanne, D. (2013). Enhanced Intrinsic Excitability in Basket Cells Maintains Excitatory-Inhibitory Balance in Hippocampal Circuits. *Neuron*, *77*, 712–722.

Cardin, J. A., Carlén, M., Meletis, K., Knoblich, U., Zhang, F., Deisseroth, K., … Moore, C. I. (2009). Driving fast-spiking cells induces gamma rhythm and controls sensory responses. *Nature*, *459*, 663–667.

Chen, J. L., Villa, K. L., Cha, J. W., So, P. T. C., Kubota, Y., & Nedivi, E. (2012). Clustered Dynamics of Inhibitory Synapses and Dendritic Spines in the Adult Neocortex. *Neuron*, *74*, 361–373.

Dehorter, N., Ciceri, G., Bartolini, G., Lim, L., del Pino, I., & Marín, O. (2015). Tuning of fast-spiking interneuron properties by an activity-dependent transcriptional switch. *Science*, *349*, 1216–1220.

Du, J., Zhang, L., Weiser, M., Rudy, B., & McBain, C. J. (1996). Developmental expression and functional characterization of the potassium-channel subunit Kv3.1b in parvalbumin-containing interneurons of the rat hippocampus. *The Journal of Neuroscience: The Official Journal of the Society for Neuroscience*, *16*, 506–518.

Espinosa, J. S., & Stryker, M. P. (2012). Development and plasticity of the primary visual cortex. *Neuron*, *75*, 230–249.

Fan, Y., Fricker, D., Brager, D. H., Chen, X., Lu, H.-C., Chitwood, R. A., & Johnston, D. (2005). Activity-dependent decrease of excitability in rat hippocampal neurons through increases in Ih. *Nature Neuroscience*, *8*, 1542–1551.

Feldman, D. E. (2009). Synaptic mechanisms for plasticity in neocortex. *Annual Review of Neuroscience*, *32*, 33–55.

Finnerty, G. T., Roberts, L. S., & Connors, B. W. (1999). Sensory experience modifies the short-term dynamics of neocortical synapses. *Nature*, *400*, 367–371.

Fox, K. (2002). Anatomical pathways and molecular mechanisms for plasticity in the barrel cortex. *Neuroscience*, *111*, 799–814.

Gainey, M. A., Aman, J. W., & Feldman, D. E. (2018). Rapid Disinhibition by Adjustment of PV Intrinsic Excitability during Whisker Map Plasticity in Mouse S1. *The Journal of Neuroscience*, *38*, 4749–4761.

Gainey, M. A., & Feldman, D. E. (2017). Multiple shared mechanisms for homeostatic plasticity in rodent somatosensory and visual cortex. *Philosophical Transactions of the Royal Society of London. Series B, Biological Sciences*, *372*, 20160157.

Gambino, F., & Holtmaat, A. (2012). Spike-Timing-Dependent Potentiation of Sensory Surround in the Somatosensory Cortex Is Facilitated by Deprivation-Mediated Disinhibition. *Neuron*, *75*, 490–502.

Goldberg, E. M., Clark, B. D., Zagha, E., Nahmani, M., Erisir, A., & Rudy, B. (2008). K+ Channels at the Axon Initial Segment Dampen Near-Threshold Excitability of Neocortical Fast-Spiking GABAergic Interneurons. *Neuron*, *58*, 387–400.

Grubb, M. S., & Burrone, J. (2010). Activity-dependent relocation of the axon initial segment fine-tunes neuronal excitability. *Nature*, *465*, 1070–1074.

Gutman, G. A., Chandy, K. G., Grissmer, S., Lazdunski, M., Mckinnon, D., Pardo, L. A., … Wang, X. (2005). International Union of Pharmacology. LIII. Nomenclature and Molecular Relationships of Voltage-Gated Potassium Channels. *Pharmacological Reviews*, *57*, 473–508.

Harauzov, A., Spolidoro, M., DiCristo, G., De Pasquale, R., Cancedda, L., Pizzorusso, T., … Maffei, L. (2010). Reducing Intracortical Inhibition in the Adult Visual Cortex Promotes Ocular Dominance Plasticity. *Journal of Neuroscience*, *30*, 361–371.

Hengen, K. B., Lambo, M. E., Van Hooser, S. D., Katz, D. B., & Turrigiano, G. G. (2013). Firing rate homeostasis in visual cortex of freely behaving rodents. *Neuron*, *80*, 335–342.

Hippenmeyer, S., Vrieseling, E., Sigrist, M., Portmann, T., Laengle, C., Ladle, D. R., & Arber, S. (2005). A developmental switch in the response of DRG neurons to ETS transcription factor signaling. *PLoS Biology*, *3*, e159.

House, D. R. C., Elstrott, J., Koh, E., Chung, J., & Feldman, D. E. (2011). Parallel regulation of feedforward inhibition and excitation during whisker map plasticity. *Neuron*, *72*, 819–831.

Isaacson, J. S., & Scanziani, M. (2011). How inhibition shapes cortical activity. *Neuron*, *72*, 231–243.

Jamann, N., Dannehl, D., Lehmann, N., Wagener, R., Thielemann, C., Schultz, C., … Engelhardt, M. (2021). Sensory input drives rapid homeostatic scaling of the axon initial segment in mouse barrel cortex. *Nature Communications*, *12*, 23.

Kameyama, K., Sohya, K., Ebina, T., Fukuda, A., Yanagawa, Y., & Tsumoto, T. (2010). Difference in Binocularity and Ocular Dominance Plasticity between GABAergic and Excitatory Cortical Neurons. *Journal of Neuroscience*, *30*, 1551–1559.

Keck, T., Scheuss, V., Jacobsen, R. I., Wierenga, C. J., Eysel, U. T., Bonhoeffer, T., & Hübener, M. (2011). Loss of Sensory Input Causes Rapid Structural Changes of Inhibitory Neurons in Adult Mouse Visual Cortex. *Neuron*, *71*, 869–882.

Khlaifia, A., Honoré, E., Artinian, J., Laplante, I., & Lacaille, J.-C. (2022). mTORC1 function in hippocampal parvalbumin interneurons: Regulation of firing and long-term potentiation of intrinsic excitability but not long-term contextual fear memory and context discrimination. *Molecular Brain*, *15*, 56.

Kuhlman, S. J., Olivas, N. D., Tring, E., Ikrar, T., Xu, X., & Trachtenberg, J. T. (2013). A disinhibitory microcircuit initiates critical-period plasticity in the visual cortex. *Nature*, *501*, 543–546.

Lau, D., Vega-Saenz de Miera, E. C., Contreras, D., Ozaita, A., Harvey, M., Chow, A., … Rudy, B. (2000). Impaired fast-spiking, suppressed cortical inhibition, and increased susceptibility to seizures in mice lacking Kv3.2 K+ channel proteins. *The Journal of Neuroscience: The Official Journal of the Society for Neuroscience*, *20*, 9071–9085.

Li, K.-X., Lu, Y.-M., Xu, Z.-H., Zhang, J., Zhu, J.-M., Zhang, J.-M., … Li, X.-M. (2012). Neuregulin 1 regulates excitability of fast-spiking neurons through Kv1.1 and acts in epilepsy. *Nature Neuroscience*, *15*, 267–273.

Li, L., Bender, K. J., Drew, P. J., Jadhav, S. P., Sylwestrak, E., & Feldman, D. E. (2009). Endocannabinoid Signaling Is Required for Development and Critical Period Plasticity of the Whisker Map in Somatosensory Cortex. *Neuron*, *64*, 537–549.

Li, L., Gainey, M. A., Goldbeck, J. E., & Feldman, D. E. (2014). Rapid homeostasis by disinhibition during whisker map plasticity. *Proceedings of the National Academy of Sciences*, *111*, 1616–1621.

Madisen, L., Zwingman, T. A., Sunkin, S. M., Oh, S. W., Zariwala, H. A., Gu, H., … Zeng, H. (2010). A robust and high-throughput Cre reporting and characterization system for the whole mouse brain. *Nature Neuroscience*, *13*, 133–140.

Marik, S. A., Yamahachi, H., McManus, J. N. J., Szabo, G., & Gilbert, C. D. (2010). Axonal Dynamics of Excitatory and Inhibitory Neurons in Somatosensory Cortex. *PLoS Biology*, *8*, e1000395.

Matsuda, Y.-T., Miyamoto, H., Joho, R. H., & Hensch, T. K. (2021). Kv3.1 channels regulate the rate of critical period plasticity. *Neuroscience Research*, *167*, 3–10.

Resnik, J., & Polley, D. B. (2017). Fast-spiking GABA circuit dynamics in the auditory cortex predict recovery of sensory processing following peripheral nerve damage. *ELife*, *6*, e21452.

Roth, F. C., & Hu, H. (2020). An axon-specific expression of HCN channels catalyzes fast action potential signaling in GABAergic interneurons. *Nature Communications*, *11*, 2248.

Rudy, B., & McBain, C. J. (2001). Kv3 channels: Voltage-gated K+ channels designed for high-frequency repetitive firing. *Trends in Neurosciences*, *24*, 517–526.

Shah, M. M. (2014). Cortical HCN channels: Function, trafficking and plasticity: Cortical HCN channels. *The Journal of Physiology*, *592*, 2711–2719.

Shao, Y. R., Isett, B. R., Miyashita, T., Chung, J., Pourzia, O., Gasperini, R. J., & Feldman, D. E. (2013). Plasticity of Recurrent L2/3 Inhibition and Gamma Oscillations by Whisker Experience. *Neuron*, *80*, 210–222.

Shin, H., & Moore, C. I. (2019). Persistent Gamma Spiking in SI Nonsensory Fast Spiking Cells Predicts Perceptual Success. *Neuron*, *103*, 1150-1163.e5.

Sun, Q.-Q. (2009). Experience-Dependent Intrinsic Plasticity in Interneurons of Barrel Cortex Layer IV. *Journal of Neurophysiology*, *102*, 2955–2973.

Sun, Y., Ikrar, T., Davis, M. F., Gong, N., Zheng, X., Luo, Z. D., … Xu, X. (2016). Neuregulin-1/ErbB4 Signaling Regulates Visual Cortical Plasticity. *Neuron*, *92*, 160–173.

Turrigiano, G. G. (2017). The dialectic of Hebb and homeostasis. *Philosophical Transactions of the Royal Society of London. Series B, Biological Sciences*, *372*, 20160258.

van Versendaal, D., Rajendran, R., Saiepour, M. H., Klooster, J., Smit-Rigter, L., Sommeijer, J.-P., … Levelt, C. N. (2012). Elimination of Inhibitory Synapses Is a Major Component of Adult Ocular Dominance Plasticity. *Neuron*, *74*, 374–383.

Villa, K. L., Berry, K. P., Subramanian, J., Cha, J. W., Oh, W. C., Kwon, H.-B., … Nedivi, E. (2016). Inhibitory Synapses Are Repeatedly Assembled and Removed at Persistent Sites In Vivo. *Neuron*, *89*, 756–769.

Wehr, M., & Zador, A. M. (2003). Balanced inhibition underlies tuning and sharpens spike timing in auditory cortex. *Nature*, *426*, 442–446.

Wen, W., & Turrigiano, G. G. (2021). Developmental Regulation of Homeostatic Plasticity in Mouse Primary Visual Cortex. *The Journal of Neuroscience: The Official Journal of the Society for Neuroscience*, *41*, 9891–9905.

Winkel, F., Ryazantseva, M., Voigt, M. B., Didio, G., Lilja, A., Llach Pou, M., … Castrén, E. (2021). Pharmacological and optical activation of TrkB in Parvalbumin interneurons regulate intrinsic states to orchestrate cortical plasticity. *Molecular Psychiatry*, *26*, 7247–7256.

Yazaki-Sugiyama, Y., Kang, S., Câteau, H., Fukai, T., & Hensch, T. K. (2009). Bidirectional plasticity in fast-spiking GABA circuits by visual experience. *Nature*, *462*, 218–221.

Yu, J., Hu, H., Agmon, A., & Svoboda, K. (2019). Recruitment of GABAergic Interneurons in the Barrel Cortex during Active Tactile Behavior. *Neuron*, *104*, 412-427.e4.

Zhang, W., & Linden, D. J. (2003). The other side of the engram: Experience-driven changes in neuronal intrinsic excitability. *Nature Reviews Neuroscience*, *4*, 885–900.

Chapter 4

Conclusion

The results from these studies advance our understanding of inhibitory circuit plasticity in somatosensory cortex (S1). In Chapter 2, we show that 1-day whisker deprivation rapidly weakens parvalbumin (PV) inhibitory circuits by decreasing PV intrinsic excitability. Underlying this change in excitability is an increase in spike threshold driven by strengthened Kv1 and A-type currents (Gainey et al., 2018). Thus, rapid inhibitory plasticity in S1 follows a different mechanism than in V1, where reduced inhibition is caused by weakened excitatory inputs to PV cells (Kuhlman et al., 2013). Whisker deprivation stabilizes the net postsynaptic potential (PSP) onto L2/3 pyramidal (PYR) cells, suggesting that PV circuits mediate rapid firing rate homeostasis in S1. PV circuits are well-positioned to monitor and control PYR firing rates, since PV cells respond to local excitatory network activity and control sensory gain in nearby pyramidal cells (Avermann, Tomm, Mateo, Gerstner, & Petersen, 2012; Atallah, Bruns, Carandini, & Scanziani, 2012).

In Chapter 3, we show that whisker deprivation can drive distinct forms of plasticity in PV cells. Unlike 1-day deprivation, 3-day deprivation decreases PV intrinsic excitability, by strengthening the mAHP. The cellular mechanisms that underlie reduced PV intrinsic excitability after 3-day deprivation remain unknown. Surprisingly, 3-day deprivation did not change PV spiking or inhibition in layer (L) 2/3 pyramidal (PYR) neurons. However, we hypothesize that this is because our stimulation method largely elicited single action potentials in PV neurons. Since L2/3 PV neurons exhibit high-frequency firing *in-vivo*, we predict that 3-day deprivation reduces PV inhibition of L2/3 PYRs.

Together, these studies show that sensory deprivation triggers rapid, homeostatic plasticity of PV inhibitory circuits in S1. Our results demonstrate that the cellular and circuit mechanisms for experience-dependent plasticity differ over time and between cortical regions, suggesting that the cerebral cortex uses a diversity of strategies to stabilize neuronal activity.

References

Atallah, B. V., Bruns, W., Carandini, M., & Scanziani, M. (2012). Parvalbumin-Expressing Interneurons Linearly Transform Cortical Responses to Visual Stimuli. *Neuron*, *73*, 159–170.

Avermann, M., Tomm, C., Mateo, C., Gerstner, W., & Petersen, C. C. H. (2012). Microcircuits of excitatory and inhibitory neurons in layer 2/3 of mouse barrel cortex. *Journal of Neurophysiology*, *107*, 3116–3134.

Gainey, M. A., Aman, J. W., & Feldman, D. E. (2018). Rapid Disinhibition by Adjustment of PV Intrinsic Excitability during Whisker Map Plasticity in Mouse S1. *The Journal of Neuroscience*, *38*, 4749–4761.

Kuhlman, S. J., Olivas, N. D., Tring, E., Ikrar, T., Xu, X., & Trachtenberg, J. T. (2013). A disinhibitory microcircuit initiates critical-period plasticity in the visual cortex. *Nature*, *501*, 543–546.

Packer, A. M., & Yuste, R. (2011). Dense, Unspecific Connectivity of Neocortical Parvalbumin-Positive Interneurons: A Canonical Microcircuit for Inhibition? *Journal of Neuroscience*, *31*, 13260–13271.